Computational Mechanics manuscript No.
(will be inserted by the editor)

WYPIWYG hyperelasticity for isotropic, compressible materials

José Crespo · Marcos Latorre · Francisco Javier Montáns

Received: date / Accepted: date

Abstract Nowadays the most common approach to model elastic behavior at large strains is through hyperelasticity. Hyperelastic models usually specify the shape of the stored energy function. This shape is modulated by some material parameters that are computed so the predicted stresses best fit the experimental data. Many stored energy functions have been proposed in the literature for isotropic and anisotropic materials, either compressible or incompressible. What-You-Prescribe-Is-What-You-Get (WYPIWYG) formulations present a different approach which may be considered an extension of the infinitesimal framework. The shape of the stored energy is not given beforehand but computed numerically from experimental data solving the equilibrium equations. The models exactly fit the experimental data without any material parameter. WYPIWYG procedures have comparable efficiency in finite element procedures as classical hyperelasticity. In this work we present a WYPIWYG numerical procedure for compressible isotropic materials and we motivate the formulation through an equivalent infinitesimal model.

José Crespo
Escuela Técnica Superior de Ingeniería Aeronáutica y del Espacio, Universidad Politécnica de Madrid
Pza.Cardenal Cisneros, 28040-Madrid, Spain
E-mail: j.crespo@upm.es

Marcos Latorre
Escuela Técnica Superior de Ingeniería Aeronáutica y del Espacio, Universidad Politécnica de Madrid
Pza.Cardenal Cisneros, 28040-Madrid, Spain
E-mail: m.latorre.ferrus@upm.es

Francisco Javier Montáns (✉)
Escuela Técnica Superior de Ingeniería Aeronáutica y del Espacio, Universidad Politécnica de Madrid
Pza.Cardenal Cisneros, 28040-Madrid, Spain
E-mail: fco.montans@upm.es

Keywords Hyperelasticity · WYPIWYG hyperelasticity · Soft materials · Polymers · Biological tissues

1 Introduction

Rubber-like solids [1–4] and soft biological materials [5, 6] are able to sustain large strains in many cases without relevant inelastic effects during loading. The behavior of these materials is frequently modelled as that of hyperelastic materials. Then, other effects may be added to the hyperelastic formulation as for example viscoelasticity or damage [1, 2, 4–6]. A hyperelastic model typically consists of an assumed stored energy function shape having some material parameters which are left free to be prescribed by the user. These material parameters are computed in such a way that the model predictions fit the available experimental data [3, 7, 8]. The typical procedure is to establish an error function between predictions and experimental data and then minimize that error employing an optimization algorithm, for example, the Levenberg-Marquardt algorithm [7, 8]. Therefore, in the current usual procedure, a stored energy is proposed (either physically motivated or purely phenomenological) and that function is modulated as to fit experimental data from different types of tests presented to the model, see for example [8–11]. The obvious purpose is to characterize the behavior of the material in any loading situation [12]. Thereafter the behavior from the resulting stored energy density is sometimes checked against the experimental data from other additional tests [13–22]. The models may be even modified in order to account for some experimental evidence [24]. This procedure is also

employed in anisotropic materials, typically in biological tissues, see for example [25–42], among many others.

The What-You-Prescribe-Is-What-You-Get (WYPIWYG) approach is very different from that employed in classical models. Instead of prescribing the shape of the stored energy, this shape is computed numerically from the presented experimental data, i.e. it is in essence a computational procedure instead of a purely analytical one. The WYPIWYG model for incompressible isotropic hyperelasticity compatible with the Valanis-Landel [43] decomposition is due to Sussman and Bathe [44]. This model uses the Kearsley and Zapas inversion formula [45] to exactly obtain the stored energy in a given number of points. Then the energy function is interpolated using piecewise cubic splines in order to have a piecewise analytical expression that may be used in a finite element program. The Sussman–Bathe WYPIWYG formulation is currently available in the commercial finite element program ADINA [46].

WYPIWYG models for incompressible transversely isotropic [47] and orthotropic materials [48] are due to Latorre and Montáns. These formulations use a generalization of the Inversion Formula and a separable form of the stored energy density similar to that of the infinitesimal framework but in functions of invariants of the logarithmic strains, which are a natural extension of the infinitesimal ones [49–52]. The numerical efficiency of these procedures in finite element implementations is similar to that of traditional models, see [46] for the isochoric, isotropic formulation and [48, 53, 54] in the context of incompressible anisotropy. The WYPIWYG procedure has been extended to viscoelasticity [53, 54] and damage [55] in order to model the Mullins effect. WYPIWYG hyperelastic functions are obtained from a set of experimental data, either from true experiments or freely prescribed by the modeler. The proposed set of experimental data is a key ingredient of the procedure, because the equations from this set are solved in a numerically exact manner in order to extract the stored energy information. The experimental set must be complete so these experiments uniquely define the behavior of the material under the constitutive assumptions. This set is equivalent to the set of material constants of a comparable infinitesimal model [56–58].

The main difficulty of WYPIWYG hyperelasticity lies in the necessity of solving the differential equations of the proposed experiments. Hence the inclusion of different material symmetries or compressibility results in necessary nontrivial modifications of the overall computational procedure, i.e. WYPIWYG hyperelasticity is not a model, but a family of computational procedures. Classical hyperelasticity proposes global solutions to the problem (as Rayleigh functions does in structural mechanics problems) and material parameters adapt that solution as to fit experimental data. On the contrary WYPIWYG hyperelasticity proposes local interpolations (as the Galerkin method does in structural mechanics) between computed, numerically exact solutions to the problem, i.e. the energy derivatives. The point is that once the stored energy is obtained solving a complete set of experiments, it is valid and accurate (if the constitutive hypotheses are fulfilled) in any other loading situation, i.e. the material behavior is completely and uniquely determined.

The purpose of this paper is to extend the WYPIWYG approach to compressible isotropic materials. The model is capable of capturing a proper complete set of experimental data that defines the material behavior up to machine precision. Because WYPIWYG approaches are a natural extension of the infinitesimal framework, in the next section we present a comparable infinitesimal bilinear model just for motivation and to explain the number of experimental curves needed to properly define the material. Thereafter, keeping an instructive parallelism with the bilinear model, we introduce the computational procedure and describe possible experiments to practically determine the large strain hyperelastic model. We also explain how to perform the equivalence to uniaxial curves which may be set as the standard input data to the model in finite element programs.

Some demonstrative examples show that the model is capable of exactly capturing some stored energy functions published in the literature (Neohookean [59], Ogden [60, 61], Mooney [62], Hartmann–Neff [63]) using only their numerical stress-strain predictions for the uniaxial test as if they were "experimental data" of a real material. Then, the behavior of these models under any arbitrary loading conditions is also captured "exactly" (numerically speaking). This shows that if the real material were behaving as these models predict, we would also capture the behavior under any arbitrary type of loading. In another example we predict the uniaxial behavior of the stored energy from Gent [64]. We note that this model does not follow the Valanis-Landel decomposition, which is one of the assumptions of our procedure. However, because the Valanis-Landel decomposition is mathematically accurate for moderate large strains [3], we show that even in this case we are able to capture to a very high precision the behavior predicted by this model in any loading situation for those moderately large strains. To show the performance of our proposal to capture the behavior observed in actual materials, we use the experiments by Blatz and Ko [65] over compressible polyurethane foam. The observed differences between our predictions

and experimental data in a different test than those used to determine the stored energies are of the order of the measured experimental errors. We note that if that were not the case, the only possibility would be that at least one of the hypotheses (isotropy, hyperelastic behavior, Valanis-Landel) would not be applicable to this material. We thereafter verify that the incompressible WYPIWYG formulation of Sussman and Bathe is recovered as a particular case in the limit. In practical finite element implementations incompressibility is frequently enforced through penalty volumetric formulations which frequently result in numerically underconstrained problems at low strains or numerical conditioning problems at large strains. Then our procedure is also a natural way of properly enforcing quasi-incompressibility in finite element simulations at every strain level, hence circumventing this problem. We also show the performance in finite element simulations and the equivalence (even in terms of iterations and convergence values) to models based on analytical functions.

Finally we note that WYPIWYG anisotropic formulations (as any other anisotropic hyperelastic model) should recover the isotropic behavior when the experimental data presented to the model is that of an isotropic material [67]. The current proposal may be coupled to our incompressible transversely isotropic and orthotropic WYPIWYG models [47, 48] as described in [67] in order to obtain a compressible orthotropic model or to obtain a quasi-incompressible one with the incompressibility constraint adequately enforced at every strain level.

2 The infinitesimal bilinear model

As mentioned, the purpose of this section is to perform a parallelism of the nonlinear model with an infinitesimal model. To facilitate the comparisons with the large strain model we will consider initially that the material has different linear behavior in extension than in compression, because as we will see the nonlinear model evaluates functions in both ranges in the same equation. Then, of course, the linearized behavior of the nonlinear formulation at the origin is recovered if we make the slopes of both branches equal.

2.1 Basic model determination

Consider a bilinear infinitesimal isotropic and compressible material which nonlinearity simply consists in that it has different linear behavior under tension and compression. Let $\boldsymbol{I}$ be the second order identity tensor and

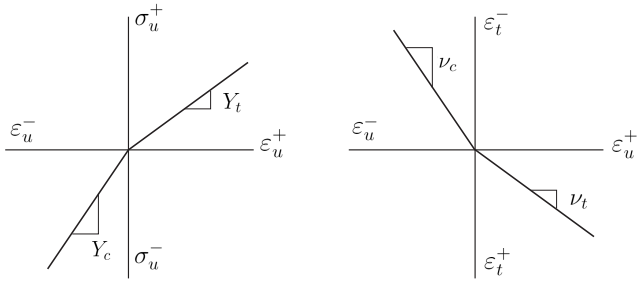

Fig. 1 Bilinear model. Left plot: stress-strain uniaxial bilinear behavior. Right plot: Transverse strains bilinear behavior.

$\mathbb{P}$ the fourth order projector tensor

$$\mathbb{P} := \mathbb{I}^s - \tfrac{1}{3}\boldsymbol{I} \otimes \boldsymbol{I} \tag{1}$$

where $\mathbb{I}^s$ is the symmetric fourth-order identity tensor. Let also $\varepsilon^v = tr(\boldsymbol{\varepsilon}) = \varepsilon_1 + \varepsilon_2 + \varepsilon_3$ be the volumetric strain and $\varepsilon_i^d = \varepsilon_i - \frac{1}{3}\varepsilon^v$ be the principal deviatoric strains, whose principal directions are $\boldsymbol{N}_i$. Then the constitutive equations may be written in uncoupled volumetric-deviatoric fashion as

$$\boldsymbol{\sigma} = \boldsymbol{\sigma}^v + \boldsymbol{\sigma}^d = K_* \varepsilon^v \boldsymbol{I} + \boldsymbol{\sigma}^{|d} : \mathbb{P} \tag{2}$$

where $\boldsymbol{\sigma}$ is the stress tensor,

$$K_* = \begin{cases} K_t & \text{if } \varepsilon^v \geq 0 \\ K_c & \text{if } \varepsilon^v < 0 \end{cases} \tag{3}$$

is the bulk modulus and $\boldsymbol{\sigma}^{|d}$ is the modified stress tensor (generally non-deviatoric if $\mu_c \neq \mu_t$)

$$\boldsymbol{\sigma}^{|d} = \sum_{i=1}^{3} \sigma_i^{|d} \boldsymbol{N}_i \otimes \boldsymbol{N}_i = \sum_{i=1}^{3} \left(2\mu_* \varepsilon_i^d\right) \boldsymbol{N}_i \otimes \boldsymbol{N}_i \tag{4}$$

such that

$$\mu_* = \begin{cases} \mu_t & \text{if } \varepsilon_i^d \geq 0 \\ \mu_c & \text{if } \varepsilon_i^d < 0 \end{cases} \tag{5}$$

Thus, we take into account the possibility of different moduli in extension and compression. Note that we have four moduli to be determined. Then we need four (linear) independent semi-curves (two extension-compression curves) to determine such moduli. Assume that by some tests we can determine the behavior of the material under tension and compression, and that the experimental data is presented in the form of a uniaxial (tension-compression) test curve $\sigma_u(\varepsilon_u)$ (Young moduli Y_t and Y_c) and a uniaxial (tension-compression) test curve $\varepsilon_t(\varepsilon_u)$ (Poisson ratios ν_t and ν_c, see Figure 1) such that the slopes are—note that the subscript t

means *transverse* in the strain variable ε_t but *tension* in the material constants Y_t, ν_t, K_t and μ_t.

$$\begin{cases} Y_t = \sigma_u^+/\varepsilon_u^+ & \text{for } \varepsilon_u^+ \geq 0 \\ Y_c = \sigma_u^-/\varepsilon_u^- & \text{for } \varepsilon_u^- < 0 \end{cases} \tag{6}$$

and

$$\begin{cases} \nu_t = -\varepsilon_t^+/\varepsilon_u^+ & \text{for } \varepsilon_u^+ \geq 0 \\ \nu_c = -\varepsilon_t^-/\varepsilon_u^- & \text{for } \varepsilon_u^- < 0 \end{cases} \tag{7}$$

We have used + and − superscripts in order to emphasize the sign of the main (driving) strain ε_u. We will use this emphasizing notation when convenient. The four experimental moduli Y_t, Y_c, ν_t, ν_c determine the basic constitutive ones K_t, K_c, μ_t and μ_c.

For example, during extension in direction 1 the strains are

$$\begin{cases} \varepsilon_1 \equiv \varepsilon_u^+ > 0 \quad \text{and} \quad \varepsilon_2 = \varepsilon_3 \equiv \varepsilon_t^+ < 0 \\ \varepsilon_u^{v+} = \varepsilon_1 + 2\varepsilon_2 > 0 \\ \varepsilon_u^{d+} \equiv \varepsilon_1^d = \frac{2}{3}(\varepsilon_1 - \varepsilon_2) > 0 \\ \varepsilon_2^d \equiv \varepsilon_3^d = -\frac{1}{3}(\varepsilon_1 - \varepsilon_2) < 0 \end{cases} \tag{8}$$

Then, the deviatoric stresses in compact Voigt notation are (just using the diagonal terms involved)

$$\boldsymbol{\sigma}^{|d} : \mathbb{P} = \begin{bmatrix} 2/3 & -1/3 & -1/3 \\ -1/3 & 2/3 & -1/3 \\ -1/3 & -1/3 & 2/3 \end{bmatrix} \begin{bmatrix} 2\mu_t \varepsilon_u^{d+} \\ 2\mu_c \varepsilon_t^{d+} \\ 2\mu_c \varepsilon_t^{d+} \end{bmatrix} \tag{9}$$

$$= \begin{bmatrix} \frac{2}{3}\left(2\mu_t \varepsilon_u^{d+} - 2\mu_c \varepsilon_t^{d+}\right) \\ -\frac{1}{3}\left(2\mu_t \varepsilon_u^{d+} - 2\mu_c \varepsilon_t^{d+}\right) \\ -\frac{1}{3}\left(2\mu_t \varepsilon_u^{d+} - 2\mu_c \varepsilon_t^{d+}\right) \end{bmatrix} \tag{10}$$

The equilibrium equations are

$$\begin{cases} \sigma_1 = K_t \varepsilon_u^{v+} + \frac{2}{3}\left(2\mu_t \varepsilon_u^{d+} - 2\mu_c \varepsilon_t^{d+}\right) \equiv \sigma_u^+ \\ 0 = K_t \varepsilon_u^{v+} - \frac{1}{3}\left(2\mu_t \varepsilon_u^{d+} - 2\mu_c \varepsilon_t^{d+}\right) \end{cases} \tag{11}$$

We can factor-out $K_t \varepsilon_u^{v+}$ from the second equation

$$K_t \varepsilon_u^{v+} = \frac{1}{3}\left(2\mu_t \varepsilon_u^{d+} - 2\mu_c \varepsilon_t^{d+}\right) \tag{12}$$

and substitute in the first one to get

$$\sigma_u^+ = \left(2\mu_t \varepsilon_u^{d+} - 2\mu_c \varepsilon_t^{d+}\right) \quad \text{with } \varepsilon_u > 0 \tag{13}$$

or —note that K_t is not involved if we measure ε_t

$$\sigma_u^+ = 2\mu_t \left[\frac{2}{3}\left(\varepsilon_u^+ - \varepsilon_t^+\right)\right] - 2\mu_c \left[-\frac{1}{3}\left(\varepsilon_u^+ - \varepsilon_t^+\right)\right] \tag{14}$$

Note also that $\varepsilon_t^d = -\frac{1}{2}\varepsilon_u^d$ and

$$\sigma_u^+ = (2\mu_t + \mu_c)\,\varepsilon_u^{d+} \;\Rightarrow\; 2\mu_t + \mu_c = \frac{\sigma_u^+}{\varepsilon_u^{d+}} \tag{15}$$

Then combining Eqs. (11) and (12) we also have

$$K_t \varepsilon_u^{v+} = \sigma_u^+/3 \tag{16}$$

i.e. if the transverse strain is given by $\varepsilon_t = -\nu_t \varepsilon_u$ we obtain the expected relation

$$K_t = \frac{\sigma_u^+}{3(1-2\nu_t)\,\varepsilon_u^+} = \frac{Y_t}{3(1-2\nu_t)} \tag{17}$$

Since $\left(\varepsilon_u^+ - \varepsilon_t^+\right) = (1+\nu_t)\,\varepsilon_u^+$, Identity $(11)_1$ can be written as

$$\sigma_1^+ = \left(\tfrac{2}{3}2\mu_t + \tfrac{1}{3}2\mu_c\right)(1+\nu_t)\,\varepsilon_u^+ \equiv Y_t \varepsilon_u^+ \tag{18}$$

so we obtain

$$\frac{1}{3}(2\mu_t + \mu_c) = \frac{Y_t}{2(1+\nu_t)} =: G_t \tag{19}$$

This relation should be familiar to the reader for the particular case $\mu_c = \mu_t$. It is evident that we need the compression part in order to fully determine the basic constitutive parameters because of the involvement of μ_c. These equations emphasize the need for the compression part to properly define the material [56].

Consider now the compression test in which the strains are

$$\begin{cases} \varepsilon_1^- \equiv \varepsilon_u^- < 0 \quad \text{and} \quad \varepsilon_2^- = \varepsilon_3^- \equiv \varepsilon_t^- > 0 \\ \varepsilon_u^{v-} = \varepsilon_1^- + 2\varepsilon_2^- < 0 \\ \varepsilon_u^{d-} \equiv \varepsilon_1^{d-} = \frac{2}{3}\left(\varepsilon_1^- - \varepsilon_2^-\right) < 0 \\ \varepsilon_2^{d-} \equiv \varepsilon_3^{d-} = -\frac{1}{3}\left(\varepsilon_1^- - \varepsilon_2^-\right) \equiv -\frac{1}{2}\varepsilon_1^{d-} > 0 \end{cases} \tag{20}$$

Performing the same algebraic manipulations as for the tension case

$$\sigma_u^- = 2\mu_c \varepsilon_u^{d-} - 2\mu_t \varepsilon_t^{d-} = (2\mu_c + \mu_t)\,\varepsilon_u^{d-} \tag{21}$$

and

$$K_c \varepsilon_u^{v-} = \sigma_u^-/3 \tag{22}$$

If the transverse strain is given by $\varepsilon_t^- = -\nu_c \varepsilon_u^-$ we obtain again the expected relation for compression

$$K_c = \frac{\sigma_u^-}{3(1-2\nu_c)\,\varepsilon_u^-} = \frac{Y_c}{3(1-2\nu_c)} \tag{23}$$

2.2 Determination of the material constants from actual tests

Whereas the tensile test is easy to perform in soft materials, an unconfined compression test is not so reliable. An alternative in incompressible materials is to substitute the compression test by an equibiaxial test, which is completely equivalent in such incompressible case [56]. However, as we will see below, in the compressible case we need an additional test in order to present a complete, independent group of experimental data. The physical reason is that in the equibiaxial test the volume also expands as in the tensile test.

Consider the equibiaxial test equilibrium equations when the stretch is in directions 1 and 2, so —we do not need the sign emphasis notation because we will assume always an equibiaxial test in extension

$$\begin{cases} \varepsilon_1 = \varepsilon_2 \equiv \varepsilon_e > 0 \quad \text{and} \quad \varepsilon_3 \equiv \varepsilon_w < 0 \\ \varepsilon_e^v = 2\varepsilon_1 + \varepsilon_3 > 0 \\ \varepsilon_1^d \equiv \varepsilon_2^d = \frac{1}{3}\left(\varepsilon_1 - \varepsilon_3\right) \equiv \varepsilon_e^d > 0 \\ \varepsilon_3^d = -\frac{2}{3}\left(\varepsilon_1 - \varepsilon_3\right) \equiv -2\varepsilon_1^d = \varepsilon_w^d < 0 \end{cases} \tag{24}$$

Then

$$\boldsymbol{\sigma}^{|d} : \mathbb{P} = \begin{bmatrix} \frac{1}{3}\left(2\mu_t\varepsilon_e^d - 2\mu_c\varepsilon_w^d\right) \\ \frac{1}{3}\left(2\mu_t\varepsilon_e^d - 2\mu_c\varepsilon_w^d\right) \\ -\frac{2}{3}\left(2\mu_t\varepsilon_e^d - 2\mu_c\varepsilon_w^d\right) \end{bmatrix} \tag{25}$$

So the equilibrium equations are

$$\sigma_e \equiv \sigma_1 = K_t\varepsilon_e^v + \tfrac{1}{3}\left(2\mu_t\varepsilon_e^d - 2\mu_c\varepsilon_w^d\right) \equiv B_t\varepsilon_e \tag{26}$$

$$0 = K_t\varepsilon_e^v - \tfrac{2}{3}\left(2\mu_t\varepsilon_e^d - 2\mu_c\varepsilon_w^d\right) \tag{27}$$

where B_t is the tensile equibiaxial stiffness modulus. Obviously we can again factor-out $K_t\,(\varepsilon_e^v)$ from the second equation

$$K_t\varepsilon_e^v = \tfrac{2}{3}\left(2\mu_t\varepsilon_e^d - 2\mu_c\varepsilon_w^d\right) \tag{28}$$

and substitute in the first equation

$$\sigma_e = 2\mu_t\varepsilon_e^d - 2\mu_c\varepsilon_w^d = 2\mu_t\varepsilon_e^d - 2\mu_c\left(-2\varepsilon_e^d\right) \tag{29}$$

$$= \left(2\mu_t + 4\mu_c\right)\varepsilon_e^d \quad \text{with } \varepsilon_e > 0 \tag{30}$$

or

$$\sigma_e = \tfrac{2}{3}\left[\mu_t\left(\varepsilon_e - \varepsilon_w\right) + 2\mu_c\left(\varepsilon_e - \varepsilon_w\right)\right] \tag{31}$$

so —cf. Eq. (16)

$$K_t\varepsilon_e^v = 2\sigma_e/3 \tag{32}$$

i.e. using $\varepsilon_e^v = \left(2 - \nu_e\right)\varepsilon_e$, where ν_e is the Poisson-like equibiaxial ratio (with value of $\nu_e = 2$ for the incompressible case)

$$K_t = \frac{B_t}{3\left(1 - \nu_e/2\right)} = \frac{Y_t}{3\left(1 - 2\nu_t\right)} \tag{33}$$

If we compare Eq. (29) with Eq. (21) we can define the uniaxial equivalence

$$\frac{-\sigma_e}{-2\varepsilon_e^d} = 2\mu_c + \mu_t = \frac{\sigma_u^-}{\varepsilon_u^{d-}} \tag{34}$$

We now use the underline notation to emphasize for future reference that they are functions with different dependency but with the same numerical value for equivalent arguments, i.e. underlined functions have deviatoric strains as arguments. We also use the bracketed subindex (u) to emphasize that they are uniaxial-equivalent values obtained from equibiaxial ones; i.e.

$$\underline{\sigma}_{(u)}^-\left(-2\varepsilon_e^d\right) = -\underline{\sigma}_e\left(\varepsilon_{(u)}^{d-}\right) \quad \text{with } \underline{\sigma}_e > 0 \text{ so } \underline{\sigma}_{(u)}^- < 0 \tag{35}$$

Note that $\varepsilon_{(u)}^{d-} = \varepsilon_w^d$, i.e. the uniaxial equivalent deviatoric strains are the transverse equibiaxial deviatoric deformations

$$\varepsilon_{(u)}^{d-} = \varepsilon_w^d = -2\varepsilon_e^d = -\tfrac{2}{3}\left(\varepsilon_e - \varepsilon_w\right) \quad \text{with } \varepsilon_{(u)} < 0 \tag{36}$$

Comparing the moduli—cf. Eq. (21)

$$\underline{\sigma}_{(u)} = -\underline{\sigma}_e = \left(\mu_t + 2\mu_c\right)\left(-2\varepsilon_e^d\right) \equiv \left(\mu_t + 2\mu_c\right)\varepsilon_{(u)}^{d-} \tag{37}$$

$$= Y_c\varepsilon_{(u)}^- = -B_t\varepsilon_e \tag{38}$$

We remark that this equivalence is established only with the deviatoric strains, i.e. $\underline{\sigma}_{(u)}^-\left(\varepsilon_{(u)}^{d-}\right)$. In order to complete the equivalence, i.e. determine $\sigma_{(u)}^-\left(\varepsilon_{(u)}^-\right)$, we need the volumetric part which we obtain below. It is immediate to show that

$$\frac{B_t}{2\left(1 + \nu_e\right)} = \frac{Y_c}{2\left(1 + \nu_c\right)} = G_c \tag{39}$$

which clearly explains that equibiaxial and compression tests are equivalent *in deviatoric terms*. On the contrary, in volumetric terms Eq. (33) shows that the equibiaxial test is equivalent to a tensile test. Then note that from the equibiaxial test we cannot obtain K_c. If we cannot assume that $K_c = K_t$, for the remaining needed test to compute K_c we can consider a confined compression test which can be easily performed in soft

materials. In this case, if we perform the test in direction 1

$$\begin{cases} \varepsilon_1 < 0 \quad \text{and} \quad \varepsilon_2 = \varepsilon_3 = 0 \\ \varepsilon^v = \varepsilon_1 < 0 \\ \varepsilon_1^d = \frac{2}{3}\varepsilon_1 < 0 \\ \varepsilon_3^d = \varepsilon_2^d = -\frac{1}{3}\varepsilon_1 > 0 \end{cases} \tag{40}$$

and

$$\boldsymbol{\sigma}^{|d} : \mathbb{P} = \begin{bmatrix} \frac{8}{9}\varepsilon_1\mu_c + \frac{4}{9}\varepsilon_1\mu_t \\ -\frac{4}{9}\varepsilon_1\mu_c - \frac{2}{9}\varepsilon_1\mu_t \\ -\frac{4}{9}\varepsilon_1\mu_c - \frac{2}{9}\varepsilon_1\mu_t \end{bmatrix} \tag{41}$$

The equilibrium equation in the main axis is

$$\sigma_1 = \left[K_c + \frac{4}{9}2\mu_c + \frac{2}{9}2\mu_t\right]\varepsilon_1 = D_c\varepsilon_1 \tag{42}$$

where D_c is the confined compressibility modulus. Then, since we already know G_c from the equibiaxial test we can factor-out K_c

$$K_c = D_c - \tfrac{4}{9}\left(2\mu_c + \mu_t\right) = D_c - \tfrac{2}{3}\left[2\mu_c\tfrac{2}{3} - 2\mu_t\left(-\tfrac{1}{3}\right)\right] \tag{43}$$

In order to complete the equivalence to the compression branch of the uniaxial test, note that using Eq. (22) and Eq. (37), we can obtain the uniaxial equivalent volumetric strain obtained from the modulus of Eq. (43) and the equivalent stresses of the equibiaxial test

$$\varepsilon_{(u)}^{v-} = K_c^{-1}\left(\underline{\sigma}_{(u)}^{-}/3\right) \tag{44}$$

Finally the equivalence is built as follows from the pairs $(\sigma_e, \varepsilon_e)$ and $(\varepsilon_w, \varepsilon_e)$

$$\left.\begin{array}{l} \varepsilon_w \to \varepsilon_e^d = \frac{1}{3}\left(\varepsilon_e - \varepsilon_w\right) \to \varepsilon_{(u)}^{d-} = -2\varepsilon_e^d \\ \sigma_e \to \underline{\sigma}_{(u)}^{-} = -\sigma_e \to \varepsilon_{(u)}^{v-} = K_c^{-1}\underline{\sigma}_{(u)}^{-}/3 \end{array}\right\} \Rightarrow \left\{\begin{array}{l} \varepsilon_{(u)}^{-} = \frac{1}{3}\varepsilon_{(u)}^{v-} + \varepsilon_{(u)}^{d-} \\ \varepsilon_{(t)}^{-} = \frac{1}{3}\varepsilon_{(u)}^{v-} - \frac{1}{2}\varepsilon_{(u)}^{d-} \end{array}\right\} \Rightarrow \left\{\begin{array}{l} \sigma_{(u)}^{-}\left(\varepsilon_{(u)}^{-}\right) \\ \varepsilon_{(t)}^{-}\left(\varepsilon_{(u)}^{-}\right) \end{array}\right. \tag{45}$$

In summary, we can choose to obtain μ_t, μ_c, K_t and K_c directly from the complete set of tests (tensile, equibiaxial and confined compression), or from the complete uniaxial curves. As a handy alternative for standard plotting and to unify the input to the codes, the former case can be converted to the latter using the described equivalence procedure.

We now extend these ideas to large strains by use of the inversion formula.

3 The inversion formula

The formulation we will introduce in the next section is solved through a generalization of the Kearsley and Zapas inversion formula which we introduced in Ref. [47]. Assume three functions $f(x)$, $g(x)$ and $h(x)$ related by

$$f(x) = g(x) - g(h(x)) \tag{46}$$

Then, we can also write

$$f(h(x)) = g(h(x)) - g(h(h(x))) \tag{47}$$

$$f(h(h(x))) = g(h(h(x))) - g(h(h(h(x)))) \tag{48}$$

$$\ldots$$

$$f\left(h^{(k)}(x)\right) = g\left(h^{(k)}(x)\right) - g\left(h^{(k+1)}(x)\right) \tag{49}$$

$$\ldots$$

where

$$h^{(k)}(x) = \underbrace{h(h(h(\ldots h(x))))}_{k \text{ times}} \tag{50}$$

is a recursive function and we define $h^{(0)}(x) = x$. Then adding $K+1$ equations

$$g(x) - g\left(h^{(K+1)}(x)\right) = \sum_{k=0}^{K} f\left(h^{(k)}(x)\right) \tag{51}$$

If $h^{(K)}(x) \to 0$ and $f(0) = 0$, the series converges up to machine precision (i.e. numerically exact) in a finite number of K addends. Equation (51) is the general inversion formula, first derived in Reference [47]. The elegant layout of the proof as given in this Section is due to Sussman, which improved our original, lengthier proof. In the case $h^{(\infty)}(x) \nrightarrow 0$, an alternative inversion formula is possible just considering

$$f\left(h^{(-1)}(x)\right) = g\left(h^{(-1)}(x)\right) - g(x) \tag{52}$$

where $h^{(-1)}(h(x)) = x$.

4 WYPIWYG isotropic compressible hyperelasticity

In this section we extend the previous concepts to large strain hyperelasticity within the What-You-Prescribe-Is-What-You-Get realm. The formulation is based on the Valanis-Landel decomposition and a volumetric decoupling in the form

$$\Psi(E_1, E_2, E_3) = \mathcal{U}(E^v) + \mathcal{W}\left(E_1^d, E_2^d, E_3^d\right) \tag{53}$$

$$= \mathcal{U}(E^v) + \omega\left(E_1^d\right) + \omega\left(E_2^d\right) + \omega\left(E_3^d\right) \tag{54}$$

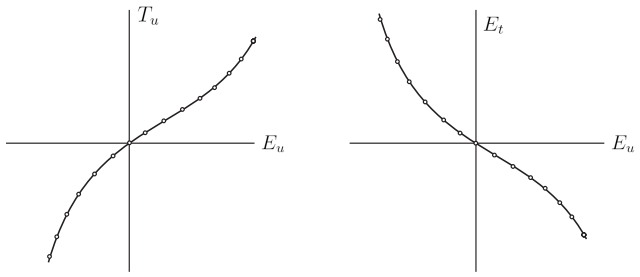

Fig. 2 Nonlinear compressible isotropic hyperelasticity. Left plot: nonlinear stress-strain behavior. Right plot: nonlinear relation between transverse and uniaxial strains. Compare with Figure 1.

where E_i are the principal logarithmic strains,

$$E^v := E_1 + E_2 + E_3 = \ln J \tag{55}$$

is the volumetric logarithmic strain (the logarithm of the Jacobian determinant J of the deformation gradient $\boldsymbol{X}$) and E_i^d are the deviatoric logarithmic strains, i.e.

$$E_i^d := E_i - \tfrac{1}{3}E^v \tag{56}$$

The (rotated or generalized [66]) Kirchhoff principal stresses are

$$\bar{\tau}_i \equiv T_i = \frac{\partial \Psi\left(E_1, E_2, E_3\right)}{\partial E_i} \tag{57}$$

$$= \frac{d\mathcal{U}\left(E^v\right)}{dE^v}\frac{\partial E^v}{\partial E_i} + \sum_{j=1}^{3}\frac{d\omega\left(E_j^d\right)}{dE_j^d}\frac{\partial E_j^d}{\partial E_i} \tag{58}$$

where

$$\frac{\partial E^v}{\partial E_i} = 1 \quad \text{and} \quad \frac{\partial E_j^d}{\partial E_i} = \delta_{ij} - \tfrac{1}{3} \tag{59}$$

In tensor notation —cf. Eq. (2)

$$\boldsymbol{T} = \boldsymbol{T}^v + \boldsymbol{T}^d = \mathcal{U}'\boldsymbol{I} + \boldsymbol{T}^{|d} : \mathbb{P} \tag{60}$$

where $\boldsymbol{T}^d := \boldsymbol{T}^{|d} : \mathbb{P}$ is the corresponding deviatoric stress tensor and $\boldsymbol{T}^{|d}$ is the modified stress tensor —cf. Eq. (4)

$$\boldsymbol{T}^{|d} := \frac{d\mathcal{W}}{d\boldsymbol{E}^d} = \sum_{i=1}^{3}\omega'\left(E_i^d\right)\boldsymbol{N}_i \otimes \boldsymbol{N}_i = \sum_{i=1}^{3} T_i^{|d}\boldsymbol{N}_i \otimes \boldsymbol{N}_i \tag{61}$$

In this equation $\boldsymbol{N}_i$ are the principal stress (and strain) directions, so $\boldsymbol{T}^{|d}$ is a second-order tensor with the same eigenvectors as $\boldsymbol{T}^d$, $\boldsymbol{T}$ and $\boldsymbol{E}$.

The purpose of the computational procedure is to obtain the stored energy derivative functions $\omega'\left(E^d\right)$ and $\mathcal{U}'\left(E^v\right)$ from some given stress-strain measured data. As we have seen in the previous section, we need to assume two complete "experimental" (prescribed by the modeller) "curves" (actually discrete pairs of data), namely $\tilde{\boldsymbol{T}}_u(\tilde{\boldsymbol{E}}_u) \equiv \tilde{\boldsymbol{\tau}}_u(\tilde{\boldsymbol{E}}_u)$ and $\tilde{\boldsymbol{E}}_t(\tilde{\boldsymbol{E}}_u)$, where $\tilde{\boldsymbol{E}}_u$ is the array of discrete, experimental, uniaxial (logarithmic) strain measurements, $\tilde{\boldsymbol{\tau}}$ is the array of corresponding Kirchhoff stresses and $\tilde{\boldsymbol{E}}_t$ is the array of corresponding transverse strains, see Figure 2, i.e. $\tilde{\tau}_p$ and $\tilde{E}_{tp}$ are the measured axial Kirchhoff stress and transverse strain at the uniaxial strain $\tilde{E}_{up}$, with $p = 1, ..., P$. We will use the *tilde* notation to denote measured experimental discrete values.

Consider the uniaxial extension test performed in direction 1 in which the driving variable is $E_u \equiv E_1$. The compatibility equations yield —cf. Eq. (8)

$$\begin{cases} E_u \equiv E_1 \quad \text{and} \quad E_t \equiv E_2 = E_3 \\ E_u^v\left(E_u\right) = E_1 + 2E_2\left(E_1\right) \\ E_u^d\left(E_u\right) \equiv E_1^d\left(E_1\right) = \frac{2}{3}\left(E_1 - E_2\left(E_1\right)\right) \\ E_t^d\left(E_u\right) = \frac{1}{3}\left(E_2\left(E_1\right) - E_1\right) = -\frac{1}{2}E_u^d\left(E_u\right) \end{cases} \tag{62}$$

so the deformation state is characterized by both the uniaxial strain E_u and the transverse strain $E_t\left(E_u\right)$, which may be a nonlinear function. The constitutive equations together with the equilibrium ones give —cf. Eq. (11)

$$\begin{cases} T_u\left(E_u\right) = \mathcal{U}'\left(E_u^v\left(E_u\right)\right) + \frac{2}{3}[\omega'\left(E_u^d\left(E_u\right)\right) - \\ \qquad\qquad -\omega'\left(E_t^d\left(E_u\right)\right)] \\ 0 = \mathcal{U}'\left(E_u^v\left(E_u\right)\right) - \frac{1}{3}\left[\omega'\left(E_u^d\left(E_u\right)\right) - \omega'\left(E_t^d\left(E_u\right)\right)\right] \end{cases} \tag{63}$$

Note that we are explicitly keeping in the notation the functional dependencies on the main, driving strain E_u. From Eq. $(63)_2$ we can factor-out $\mathcal{U}'\left(E_u^v\left(E_u\right)\right)$—cf. Eq. (12)

$$\mathcal{U}'\left(E_u^v\left(E_u\right)\right) = \tfrac{1}{3}\left[\omega'\left(E_u^d\left(E_u\right)\right) - \omega'\left(E_t^d\left(E_u\right)\right)\right] \tag{64}$$

and substitute into Eq. $(63)_1$ to obtain

$$T_u\left(E_u\right) = \omega'\left(E_u^d\left(E_u\right)\right) - \omega'\left(E_t^d\left(E_u\right)\right) \tag{65}$$

Equation (65) can be compared to Eq. (13), see interpretation in Figure 3. Note that Eq. (13) is the linearized model if we take $2\mu_c = 2\mu_t = 2\mu$, i.e. the slope of ω' at the origin. In fact $\omega''/2$ presents the evolution of the instantaneous shear modulus at each deviatoric strain value. Because of the assumed one-to-one relation in Eq. $(62)_3$ between E_u^d and E_u for this test we can define the new functional dependence $\underline{T}_u\left(E_u^d\left(E_u\right)\right)$

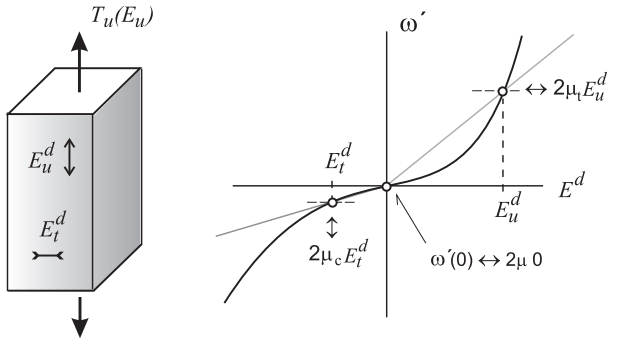

Fig. 3 Conceptual comparison of the nonlinear model with the bilinear one. The slope of ω' at the origin is the linearized modulus 2μ. The curve ω'' represents the evolution of such modulus.

$= T_u(E_u)$, numerically equal for different arguments, so now we have the same dependences

$$\underline{T}_u\left(E_u^d(E_u)\right) = \omega'\left(E_u^d(E_u)\right) - \omega'\left(-\tfrac{1}{2}E_u^d(E_u)\right) \quad (66)$$

i.e.—cf. Eq. (13)

$$\underline{T}_u\left(\tfrac{2}{3}(E_u - E_t)\right) = \omega'\left(\tfrac{2}{3}(E_u - E_t)\right) - \omega'\left(-\tfrac{1}{3}(E_u - E_t)\right) \quad (67)$$

Then, we can also determine $\mathcal{U}'$ as—cf. Eq. (16)

$$\begin{aligned}\mathcal{U}'\left(E_u^v(E_u)\right) &= \tfrac{1}{3}\left[\omega'\left(E_u^d(E_u)\right) - \omega'\left(E_t^d(E_u)\right)\right] \\ &= T_u(E_u)/3\end{aligned} \quad (68)$$

Note that $\mathcal{U}'\left(E_u^v(E_u)\right) = \mathcal{U}'\left(E_u + 2E_t(E_u)\right)$ is determined directly from $T_u(E_u)$ with the knowledge of $E_t(E_u)$. On the other hand, the function $\omega'\left(E^d\right)$ in Eq. (66) may be obtained at $E_u^d(E_u)$ from the Inversion Formula Eq. (51) as

$$\omega'\left(E_u^d(E_u)\right) = \sum_{k=0}^{K} \underline{T}_u\left(\left(-\tfrac{1}{2}\right)^k E_u^d(E_u)\right) \quad (69)$$

We have set the reference at $T_u(0) = 0$ and $\omega'(0) = 0$ —note that the actual value of $\omega'(0)$ in the previous equations is not relevant.

The relation $E_t(E_u)$ has already been used in the computation of $\underline{T}_u\left(E_u^d(E_u)\right)$. Note that T_u may be obtained from the tensile-test nominal stresses P_u as $P_u = T_u/\lambda_u = T_u \exp(-E_u)$. It is also important to note that both the tension and the compression parts of the uniaxial test are needed in Eq. (69) to determine ω', see Ref. [56]. The need for the compression data includes herein the additional data for the relation $E_t(E_u < 0)$ as to properly evaluate $E_u^d(E_u)$ for $E_u < 0$. Furthermore, this expression needs the evaluation of T_u at different values of E_u which are not necessarily coincident with those given by the experimental (discrete) data points $\tilde{E}_u$. Hence, some kind of interpolation is needed.

We use piece-wise cubic splines in order to interpolate the data sets $\tilde{\boldsymbol{T}}_u(\tilde{\boldsymbol{E}}_u)$ and $\tilde{\boldsymbol{E}}_t(\tilde{\boldsymbol{E}}_u)$. With these interpolations we obtain smooth piecewise continuous functions $T_u(E_u)$ and $E_t(E_u)$. If the experimental data present some dispersion, but we require the functions $T_u(E_u)$ and $E_t(E_u)$ to have some degree of smoothness, the "experimental" spline functions would not necessarily pass through the truly measured data points $\tilde{\boldsymbol{T}}_u(\tilde{\boldsymbol{E}}_u)$ and $\tilde{\boldsymbol{E}}_t(\tilde{\boldsymbol{E}}_u)$. We remark that the resulting smooth functions $T_u(E_u)$ and $E_t(E_u)$ constitute the actual "experimental" data *prescribed* by the user and *gotten* by the WY**P**IWY**G** procedure. Subsequently, a new discretized domain $\bar{\boldsymbol{E}}_u$ is employed (say 50 equispaced $\bar{E}_{up}$, $p = 1, .., 50$ points) in order to obtain the respective volumetric and deviatoric strain point sets $\bar{\boldsymbol{E}}_u^d$ and $\bar{\boldsymbol{E}}_u^v$ using the smoothed spline function $E_t(E_u)$, see Eqs. $(62)_2$ and $(62)_3$, and the corresponding stress point set $\bar{\boldsymbol{T}}_u$ using the smoothed spline function $T_u(E_u)$. We note that the strain point sets $\bar{\boldsymbol{E}}_u^d$ and $\bar{\boldsymbol{E}}_u^v$ are not equispaced if $E_t(E_u)$ is non linear, so further independent discretizations may be considered. With the pairs $\{\bar{\boldsymbol{E}}_u^v, \bar{\boldsymbol{T}}_u/3\}$ we directly compute the discrete solution values $\bar{\boldsymbol{U}}'(\bar{\boldsymbol{E}}_u^v)$ from Eq. (68). With the pairs $\{\bar{\boldsymbol{E}}_u^d, \bar{\boldsymbol{T}}_u\}$ we build the non-uniform spline $\underline{T}_u\left(E_u^d\right)$, which is to be used in the inversion formula of Eq. (69) in order to compute the discrete solution values $\bar{\boldsymbol{\omega}}'(\bar{\boldsymbol{E}}_u^v) \equiv \bar{\boldsymbol{T}}^{|d}(\bar{\boldsymbol{E}}_u^v)$. Once the data point sets $\bar{\boldsymbol{U}}'(\bar{\boldsymbol{E}}_u^v)$ and $\bar{\boldsymbol{\omega}}'(\bar{\boldsymbol{E}}_u^d)$ are known, the piecewise spline interpolations $\mathcal{U}'(E^v)$ and $\omega'\left(E^d\right)$ are performed, which should be re-built in order to obtain the final uniform first-derivative spline functions. Note that the impact of using piecewise splines in actual finite element simulations is negligible in terms of computational time if their domain breaks are evenly spaced because the corresponding cubic spline may be directly addressed. The stored energy first-derivative functions are determined before running any finite element simulation and then their spline coefficients are saved in memory. The memory needs to save the piecewise spline coefficients are the main disadvantage of WYPIWYG procedures. However, this memory necesity is a very low share of the memory used in a typical finite element problem.

The overall computational procedure is

$$\left.\begin{array}{c}\text{Experim.}\\ \text{data pairs:}\\ \left\{\tilde{\boldsymbol{E}}_u, \tilde{\boldsymbol{T}}_u\right\}\\ \left\{\tilde{\boldsymbol{E}}_u, \tilde{\boldsymbol{E}}_t\right\}\end{array}\right\} \xrightarrow[\text{splines}]{\text{Smooth}} \left.\begin{array}{c}\text{Spline funct.:}\\ T_u(E_u)\\ E_t(E_u)\end{array}\right\} \xrightarrow[\text{at each } \bar{E}_{up}]{\text{Eq. (62)}}$$

$$\longrightarrow \left.\begin{array}{c}\text{Resampled}\\ \text{pairs(*):}\\ \left\{\bar{\boldsymbol{E}}_u, \bar{\boldsymbol{T}}_u\right\}\\ \left\{\bar{\boldsymbol{E}}_u, \bar{\boldsymbol{E}}_u^v\right\}\\ \left\{\bar{\boldsymbol{E}}_u, \bar{\boldsymbol{E}}_u^d\right\}\end{array}\right\} \underset{\text{interp.}}{\overset{\text{Spline}}{\longrightarrow}} \left.\begin{array}{c}\text{New spline funct.:}\\ \underline{T}_u\left(E_u^d\right)\end{array}\right\} \longrightarrow$$

$$\underset{\text{at each } \bar{E}_{up},\ \text{using also (*)}}{\overset{\text{Eqs. (68) \& (69)}}{\longrightarrow}} \left.\begin{array}{c}\left\{\bar{\boldsymbol{E}}_u^v, \bar{\boldsymbol{U}}'\right\}\\ \left\{\bar{\boldsymbol{E}}_u^d, \bar{\boldsymbol{\omega}}'\right\}\end{array}\right\} \underset{\text{interp.}}{\overset{\text{Spline}}{\longrightarrow}} \left.\begin{array}{c}\mathcal{U}'\left(E^v\right)\\ \omega'\left(E^d\right)\end{array}\right\}$$

A more detailed explanation of the WYPIWYG procedures layout may be found in Ref. [48], so we omit here those details.

Note that once determined, $\mathcal{U}'\left(E^v\right)$ and $\omega'\left(E^d\right)$ uniquely define the behavior of the material in any loading situation if it fulfills the constitutive assumptions. In this general loading case, it simply suffices to obtain the stretch tensor $\boldsymbol{U}$ of the deformation gradient $\boldsymbol{X}$, extract the eigenvectors $\boldsymbol{N}_i$ and eigenvalues λ_i, define the logarithmic strains $E_i = \ln\lambda_i$, compute the volumetric and deviatoric parts using Eqs. (55) and (56), and apply Eq. (58) to obtain the principal stresses T_i or Eq. (60) to obtain $\boldsymbol{T}$.

As mentioned, since in soft materials it is usually difficult to perform accurate uniaxial compression tests, it is frequently the case when alternative tests are devised. In the next section we show how to convert data from the more convenient equibiaxial and confined uniaxial tests to the compression branch of the uniaxial tensile test.

5 Conversion of equibiaxial and confined compression test data to uniaxial data

The strains during an equibiaxial test in axes 1 and 2, with $E_1 > 0$, are

$$\begin{cases} E_e^v\left(E_1\right) = 2E_1 + E_3\left(E_1\right) > 0\\ E_e^d\left(E_1\right) \equiv E_1^d\left(E_1\right) = \frac{1}{3}\left[E_1 - E_3\left(E_1\right)\right] > 0\\ E_w^d\left(E_1\right) \equiv -\frac{2}{3}\left[E_1 - E_3\left(E_1\right)\right] \equiv -2E_1^d\left(E_1\right) < 0 \end{cases} \tag{70}$$

The equibiaxial test equilibrium and constitutive equations under the aforementioned hypotheses (isotropy and Valanis-Landel form) are

$$\begin{cases} T_1\left(E_1\right) = \mathcal{U}'\left(E_e^v\left(E_e\right)\right) + \frac{1}{3}[\omega'\left(E_e^d\left(E_e\right)\right)\\ \qquad\qquad -\omega'\left(E_w^d\left(E_e\right)\right)] \equiv T_e\left(E_e\right)\\ T_2\left(E_2\right) = ... \equiv T_e\left(E_e\right)\\ T_3 \equiv 0 = \mathcal{U}'\left(E_e^v\left(E_e\right)\right) - \frac{2}{3}\omega'\left(E_e^d\left(E_e\right)\right)\\ \qquad\qquad -\omega'\left(E_w^d\left(E_e\right)\right)] \end{cases} \tag{71}$$

From the third equation we can factor out —cf. Eq. (28)

$$\mathcal{U}'\left(E_e^v\left(E_e\right)\right) = \tfrac{2}{3}\left[\omega'\left(E_e^d\left(E_e\right)\right) - \omega'\left(E_w^d\left(E_e\right)\right)\right] \tag{72}$$

and using the first equation —cf. Eq. (32)

$$\mathcal{U}'\left(E_e^v\left(E_e\right)\right) = 2T_e\left(E_e\right)/3 \tag{73}$$

Note that $E_e^v\left(E_e\right)$ is computed from E_e and from the measured $E_w\left(E_e\right)$. On the other hand, Eqs. (70) and (73) also bring

$$T_e\left(E_e\right) = \omega'\left(E_e^d\left(E_e\right)\right) - \omega'\left(-2E_e^d\left(E_e\right)\right) \tag{74}$$

Compare this equation with Identity $(29)_2$ and note again that the linearized case is obtained for $2\mu_t = 2\mu_c = 2\mu$, where 2μ is the tangent of ω' at the origin. Defining a new function $\underline{T}_e\left(E_e^d\left(E_e\right)\right) = T_e\left(E_e\right)$,

$$\underline{T}_e\left(E_e^d\left(E_e\right)\right) = \omega'\left(E_e^d\left(E_e\right)\right) - \omega'\left(-2E_e^d\left(E_e\right)\right) \tag{75}$$

If we perform the same conversions as we did in the infinitesimal model, with $E_e \geq 0$, so $E_{(u)}^{d-} \leq 0$, we have

$$E_{(u)}^{d-}\left(E_e\right) = E_w^d\left(E_e\right) = -2E_e^d\left(E_e\right) = -\tfrac{2}{3}\left[E_e - E_w\left(E_e\right)\right] \tag{76}$$

and —cf. Eq. (35)

$$\underline{T}_{(u)}^{-}\left(-2E_e^d\left(E_e\right)\right) = -\underline{T}_e\left(E_{(u)}^{d-}\left(E_e\right)\right) \tag{77}$$

with $\underline{T}_e \geq 0$ so $\underline{T}_{(u)} < 0$. Thus we can write

$$\underline{T}_{(u)}^{-}\left(E_{(u)}^{d-}\left(E_e\right)\right) = \omega'\left(E_{(u)}^{d-}\left(E_e\right)\right) - \omega'\left(-\tfrac{1}{2}E_{(u)}^{d-}\left(E_e\right)\right) \tag{78}$$

This equation can be compared to Eq. (66), whose solution is given in Eq. (69), i.e. for $E_{(u)}^{d-} < 0$

$$\omega'\left(E_{(u)}^{d-}\left(E_e\right)\right) = \sum_{k=0}^{K} \underline{T}_u^{-}\left(\left(-\tfrac{1}{2}\right)^k E_{(u)}^{d-}\left(E_e\right)\right) \tag{79}$$

which is identical to that of the extension branch. Then, it is sufficient to apply Equivalences (76) and (77) to the experimental data and we recover the (*stem*) case of the previous section. However note that as it happened with the infinitesimal formulation, we still have not completely defined the transformation because we need the volumetric part to obtain $E_{(u)}^{-}$.

On the other hand we have only defined $\mathcal{U}'\left(E^v\right)$ for $E^v \geq 0$ because the sign in the volumetric change in both the tensile and equibiaxial tests is the same — recall the bilinear case, Eq. (39). For a general loading

situation in which volumetric compression may be expected, we need to define $\mathcal{U}'(E^v)$ for $E^v < 0$ or otherwise make a reasonable assumption on it. We also need this correspondence to complete the transformation of the experimental data to the compression branch of the uniaxial (tensile) test.

In the confined compression test in direction 1, the strain field is given by $E_1 \equiv E_c \leq 0$ and $E_2 = E_3 = 0$. Then

$$\begin{cases} E^v(E_c) = E_c \\ E_1^d(E_c) = \frac{2}{3}E_c \\ E_2^d(E_c) \equiv -\frac{1}{3}E_c \equiv E_3^d(E_c) \end{cases} \tag{80}$$

and the first equation gives —cf. Identity $(43)_2$

$$\mathcal{U}'(E_c) = T_c(E_c) - \tfrac{2}{3}\left[\omega'\left(\tfrac{2}{3}E_c\right) - \omega'\left(-\tfrac{1}{3}E_c\right)\right] \tag{81}$$

Since the last addend is already known from the tensile and equibiaxial tests, $T_c(E_c)$ determines $\mathcal{U}'(E_c)$ for values $E_c \equiv E^v \leq 0$.

Now, with the knowledge of $\mathcal{U}'(E^v)$ for $E^v \leq 0$ we can complete the equivalence computing the uniaxial transverse strains $E_{(t)}\left(E_{(u)}\right)$ for $E_{(u)} \leq 0$. Indeed Eq. (68) brings —cf. Eq. (44)

$$E_{(u)}^{v-}\left(E_{(u)}^{-}\right) = \mathcal{U}'^{(-1)}\left(\tfrac{1}{3}\underline{T}_{(u)}^{-}\right) \tag{82}$$

where $\mathcal{U}'^{(-1)}$ denotes the inverse function of $\mathcal{U}'$ (i.e. such that $\mathcal{U}'^{(-1)}\mathcal{U}'(*) = *$) which is easily performed within the piecewise spline context. Note the dependencies $\underline{T}_{(u)}^{-}\left(E_{(u)}^{d-}\left(E_{(u)}^{-}\right)\right)$. Using Eq. $(62)_2$

$$E_{(t)}^{-}\left(E_{(u)}^{-}\right) = \frac{1}{2}\left[E_{(u)}^{v-}\left(E_{(u)}^{-}\right) - E_{(u)}^{-}\right] \tag{83}$$

Then, the computational procedure is summarized as in (45)

$$\left.\begin{array}{c} E_w(E_e) \to E_e^d = \frac{1}{3}(E_e - E_w(E_e)) \to E_{(u)}^{d-} = -2E_e^d \\ T_e(E_e) \to \underline{T}_{(u)}^{-} = -T_e \to E_{(u)}^{v-} = \mathcal{U}'^{(-1)}\left(\frac{1}{3}\underline{T}_{(u)}^{-}\right) \end{array}\right\}$$
$$\Rightarrow \left\{\begin{array}{l} E_{(u)}^{-} = \frac{1}{3}E_{(u)}^{v-} + E_{(u)}^{d-} \\ E_{(t)}^{-} = \frac{1}{3}E_{(u)}^{v-} - \frac{1}{2}E_{(u)}^{d-} \end{array}\right\} \Rightarrow \left\{\begin{array}{l} T_{(u)}^{-}\left(E_{(u)}^{-}\right) \\ E_{(t)}^{-}\left(E_{(u)}^{-}\right) \end{array}\right. \tag{84}$$

6 Tangent moduli

Once the stored energy density function derivatives $\mathcal{U}'$ and ω' have been obtained, the tangent moduli are exactly the same as in any formulation employing the compressible Valanis-Landel decomposition. The tangent moduli may be easily obtained in $\boldsymbol{T} - \boldsymbol{E}$ form and then converted to any other pair of stress-strain measures through the adequate mapping tensors [66]. In general, using Eq. (54) the stress tensor $\boldsymbol{T} = \boldsymbol{T}^v + \boldsymbol{T}^d$ may be obtained as in Eq. (60). Then, using —see for example [55]

$$\mathbb{C}^{|d} := \frac{d\boldsymbol{T}^{|d}}{d\boldsymbol{E}^d} = \frac{d^2\mathcal{W}}{d\boldsymbol{E}^d d\boldsymbol{E}^d}$$
$$= \sum_{i=1}^{3}\omega''\left(E_i^d\right)\boldsymbol{M}_i \otimes \boldsymbol{M}_i + \sum_{i=1}^{3}\sum_{j\neq i}\frac{T_j^d - T_i^d}{E_j^d - E_j^d}\boldsymbol{M}_{ij} \otimes \boldsymbol{M}_{ij} \tag{85}$$

with

$$\boldsymbol{M}_i := \boldsymbol{N}_i \otimes \boldsymbol{N}_i \;\text{ and }\; \boldsymbol{M}_{ij} := \tfrac{1}{2}\left(\boldsymbol{N}_i \otimes \boldsymbol{N}_j + \boldsymbol{N}_j \otimes \boldsymbol{N}_i\right) \tag{86}$$

the constitutive tangent is obtained as

$$\mathbb{C} = \frac{d\boldsymbol{T}}{d\boldsymbol{E}} = \frac{d^2\Psi}{d\boldsymbol{E}d\boldsymbol{E}} = \mathcal{U}''(E^v)\,\boldsymbol{I} \otimes \boldsymbol{I} + \mathbb{P} : \mathbb{C}^{|d} : \mathbb{P} \tag{87}$$

Note that the derivatives of the stored energy function densities are spline derivatives (i.e. local polynomials). WYPIWYG models have comparable efficiency to traditional hyperelastic models in finite element simulations; see Ref. [48].

To finish the presentation of the procedure, it is worth mentioning that since WYPIWYG procedures are different from traditional ones in that they have no global material parameters, analyzing the stability properties of the obtained stored energy needs also different approaches in general. Of course the positive sign of the second derivatives of the corresponding energy terms ω and $\mathcal{U}$ may be readily performed once the coefficients of the splines have been computed. Restrictions on those coefficients may also be imposed in order to guarantee some stability properties. However we note that What-You-*Prescribe*-Is-What-You-*Get* procedures would be able to capture unstable behavior in unstable materials. The main concern here is that experimental noise or simultaneous presentation of data from different specimens may result in oscillatory or in nonphysical unstable predicted behavior for stable materials. Smoothing techniques for splines to fit very noisy experimental data with a given degree of smoothness or behavioral conditions are well known in statistics and in the curve and surface fitting fields, see for example [69–71] and therein references. However, in practice, normal experimental noise is easily smoothed out using penalized splines as the ones implemented in MATLAB. WYPIWYG procedures are then initialized with those pre-processed data points as prescribed input. For example we have used these splines in the computations

from actual experimental data of compressible foam in Fig. 12 below, in the computations in Ref. [56] using actual experimental data from incompressible rubber, and in the computations in Ref. [58] with data from murine skin using the incompressible transversely isotropic model. Since in these cases there was a low experimental noise, very low smoothing was needed in practice.

7 Examples

As mentioned, the model captures to any desired numerical precision the behavior of hyperelastic materials which fulfill the separability hypothesis of the strain energy function proposed by Valanis and Landel, i.e. models fulfilling the form of Eq. (54). There are many analytical stored energy functions published in the literature which follow this assumption. For the isochoric part ω we have chosen the Neohookean model [59], the Mooney model [62] and the Ogden model [60], [61]. For the volumetric part we have chosen the same function for all models which is the convex function from Hartmann and Neff [63], see arguments for the selection therein. We now show that the proposed formulation is of course capable of reproducing the behavior predicted by those models in any loading situation just employing as input the "experimental" stress-strain data that those energy functions generate for the uniaxial case. We also employ the Gent [64] model which does not follow the Valanis-Landel decomposition. We show that even in this case we are able to capture the behavior of the model to high precision in moderately large strains. Note that the Valanis-Landel decomposition is mathematically accurate for moderate large strains and has been experimentally verified in some materials [3]. Furthermore, if the real material does not follow the Valanis-Landel decomposition, additional tests are needed in order to determine the coupling between strain components at very large strains. Then we select some experimental data from Blatz and Ko [65] to show the performance of our proposal in predicting the behavior of actual materials. We also show that this formulation includes the formulation of Sussman and Bathe for isotropic (quasi-)incompressible materials as a particular case. Finally, we present a finite element simulation to show the efficiency of the method.

7.1 Volumetric component

As mentioned, for the volumetric part to be added to all models, we have chosen the function from Hartmann and Neff [63] given by the following derivative

$$\mathcal{U}'\left(E^v\right) = \frac{K}{\beta_1}\left(\exp\left(\beta_2 E^v\right) - \exp\left(\beta_3 E^v\right)\right) \tag{88}$$

where $K = 8 \times 10^5\,\mathrm{Pa}$, $\beta_1 = 10$, $\beta_2 = 4$ and $\beta_3 = -6$. The value of K was selected to allow a high compressibility at low strain as to show the features of the model. At very large strains the volumetric term usually becomes dominant. The rest of the parameters are those given by Hartmann and Neff in Table 4 of Ref. [63].

7.2 Neohookean model

The compressible Neohookean stored energy function is frequently given by the following expression [60], [59]

$$\Psi = \mathcal{U}\left(E^v\right) + C_1\left(I_1^d - 3\right) \tag{89}$$

where I_1^d is the first invariant of the isochoric (deviatoric) right Cauchy-Green deformation tensor obtained from the isochoric deformation gradient of Flory's decomposition. The material parameter is $C_1 = 0.4\,\mathrm{MPa}$, taken from Ref. [59].

For the uniaxial case, $\sigma_2 = \sigma_3 = 0$, and the problem is solved using a Newton-Raphson algorithm. Since the procedure is well-known we omit the details.

In Figure 4a we represent the uniaxial stress-strain curve, where we show the analytical predictions given by the Neohookean/Hartmann–Neff model. We have used this Neohookean predictions as the input data of our model, as if they were measured experimental data. In the same figure 4a we also show the numerical predictions using our proposal which are coincident with the spline interpolation, and the latter obviously with the predictions of the Neohookean model. In Figure 4b we show the transverse strain predictions from the Neohookean model (and also input data to our procedure) and the resulting numerical predictions using our proposal. In Figure 4c and Figure 4d we show, respectively, the stored energies derivatives ω' and $\mathcal{U}'$ for both the Neohookean/Hartmann-Neff model and the WYPIWYG model. It can be seen in this Figure that both stored energy derivatives are visually coincident. As a consequence, both predictions are also coincident. However we remark that even though the stored energy derivatives in Figures 4c and 4d look identical for both models, they are indeed different. The stored energy derivatives of the Neohookean/Hartmann–Neff model are those given by the derivative of Eqs. (89) and (88). On the contrary, the stored energy derivatives of the WYPIWYG procedure are piecewise third order polynomials. Both stored energy derivatives are exactly coincident at the discretization points $\bar{E}_{up}$.

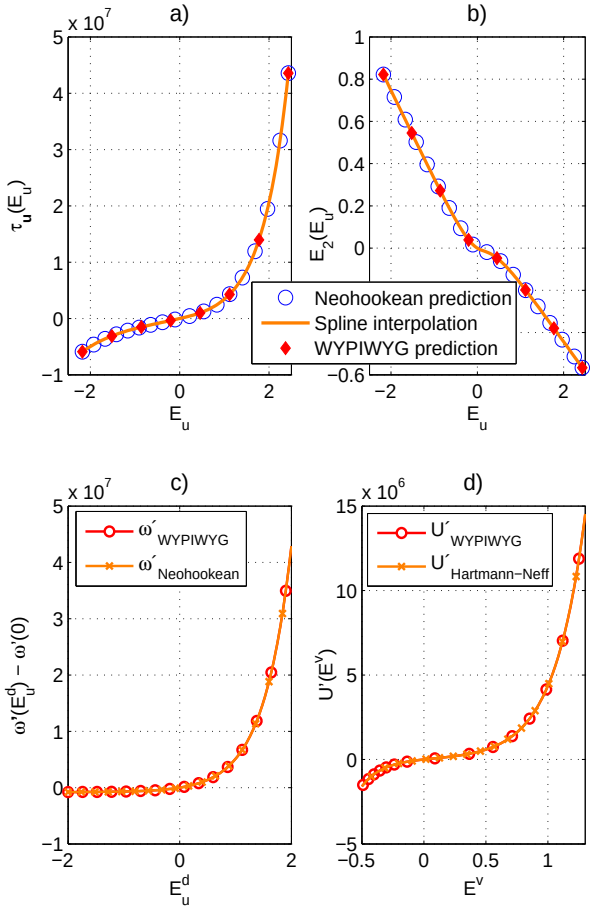

Fig. 4 Compressible Neohookean/Hartmann–Neff model predictions for the uniaxial test and WYPIWYG predictions using the former ones as "experimental" data. a) Tensile Kirchhoff stresses in Pa versus uniaxial (longidutinal) logarithmic strains. b) Transverse strains versus longitudinal strains. c) Energy derivative components ω' in Pa versus deviatoric longitudinal strains: prescribed (Neohookean) and obtained (WYPIWYG) energies. d) Volumetric stored energy derivative: prescribed (Hartmann and Neff) and obtained (WYPIWYG) energies.

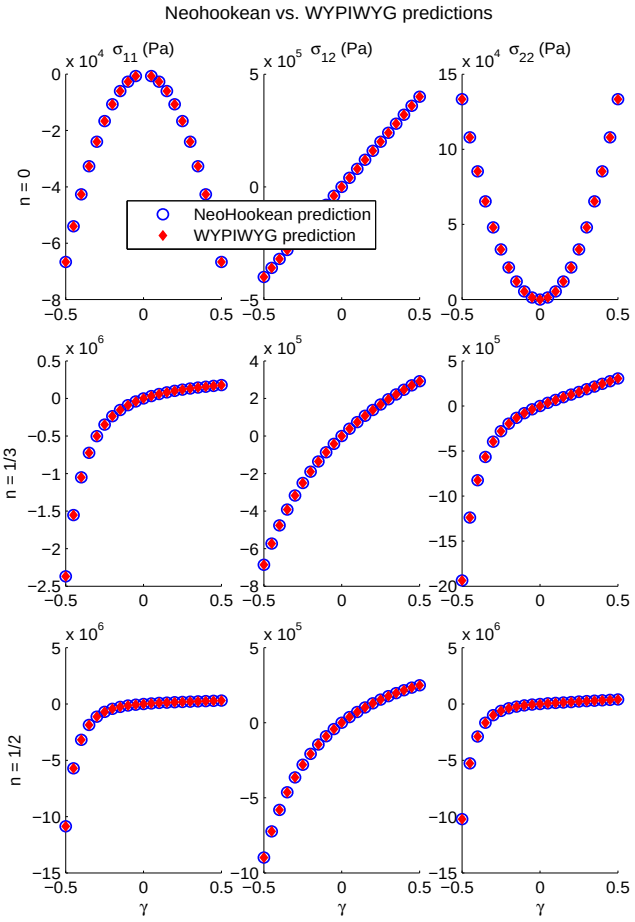

Fig. 5 Predictions for the deformation gradient given in Eq. (90) using the compressible Neohookean/Hartmann–Neff model and predictions obtained using the WYPIWYG model using the stored energies of Figure 4. First row: predictions for components σ_{11}, σ_{12}, σ_{22} (Pa) versus γ for $n = 0$ (simple shear) in Eq. (4). Second row: predictions for $n = 1/3$. Third row: predictions for $n = 1/2$.

Consider now the following family of deformation gradients

$$\boldsymbol{X} = \begin{bmatrix} (1+\gamma)^n & & \\ \gamma & (1+\gamma)^n & \\ & & 1 \end{bmatrix} \tag{90}$$

where γ is the main deformation variable and n is a constant. The case $n = 0$ is a simple shear case and γ is the "amount of shear". We consider also the cases of $n = 1/3$ and $n = 1/2$, which correspond to different combinations of volumetric and isochoric parts.

The predictions for the in-plane normal stresses σ_{11}, σ_{22} and shear stress σ_{12} as a function of the "amount of shear" γ are given in Figure 5 for both models. In this figure, as well as in similar figures below, we plot in the first row of axes the predictions for $n = 0$ in Eq. (90) (simple shear case), in the second row of axes we plot the predictions for $n = 1/3$ and in the third row of axes the predictions for $n = 1/2$. The first column corresponds to the component σ_{11} of the Cauchy stress tensor for each case, the second column corresponds to the shear component σ_{12} of the Cauchy stress tensor and in the third column the component σ_{22} of the same tensor is given. Note that in this case for the WYPIWYG model we simply use the stored energy derivatives given in Figures 4c and 4d. It should be of no surprise that the predictions using both models are coincident again in all cases. In fact, since we have "exactly" computed the stored energy, both models match

numerically and the predictions will be coincident *in any loading situation*. In the next examples we repeat these same curves, showing that we obtain the same conclusions for any model being used if it fulfills the Valanis-Landel decomposition.

7.3 Mooney model

The Mooney stored energy function is [62]

$$\Psi = \mathcal{U}\left(E^v\right) + C_1\left(I_1^d - 3\right) + C_2\left(I_2^d - 3\right) \tag{91}$$

where $C_1 = 0.39\times10^6\,\mathrm{Pa}$ and $C_2 = 0.15\times10^6\,\mathrm{Pa}$ are the material parameters, I_2^d is the second invariant of the deviatoric right Cauchy-Green deformation tensor and $\mathcal{U}\left(E^v\right)$ is the same Hartmann-Neff volumetric stored energy.

Figure 6 shows the comparison of this model and the WYPIWYG approach for the material parameters of the Mooney model. As with the previous model, it can be verified that both models give exactly the same predictions. Figure 7 shows the predictions for the deformation pattern given by Eq. (90) following the layout already explained in the previous example. It can be seen again that both models give exactly the same predictions, i.e. the WYPIWYG model exactly (numerically speaking) replicates the material behavior in any loading situation.

7.4 Ogden model

The stored energy function of the Ogden model is given by the following expression [60], [61]

$$\Psi = \mathcal{U}\left(E^v\right) + \sum_{p=1}^{M}\frac{\mu_p}{\alpha_p}\left((\lambda_1^d)^{\alpha_p} + (\lambda_2^d)^{\alpha_p} + (\lambda_3^d)^{\alpha_p} - 3\right) \tag{92}$$

where μ_i and α_i are the material parameters, M is the number of terms, typically $M = 3$, and λ_i^d are the isochoric (deviatoric) stretches. The material parameters we have used are [59] $\mu_1 = 0.62\times10^6\,\mathrm{Pa}$, $\mu_2 = 1.18\times10^3\,\mathrm{Pa}$, $\mu_3 = -9.81\times10^3\,\mathrm{Pa}$ and $\alpha_1 = 1.3$, $\alpha_2 = 5$, $\alpha_3 = -2$.

Figures 8 and 9 show the same comparisons as before. We obtain the same conclusions as in the previous examples.

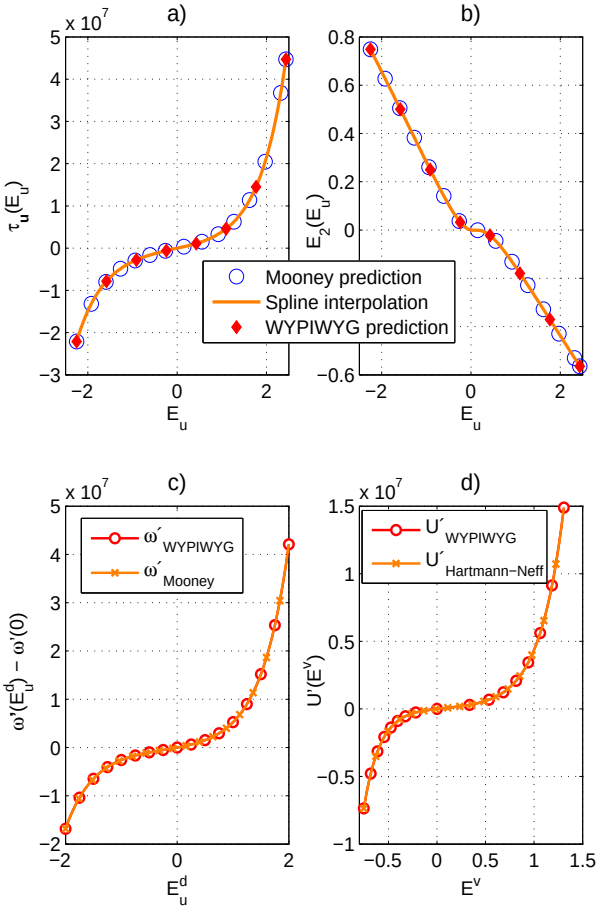

Fig. 6 Compressible Mooney/Hartmann–Neff model predictions for the uniaxial test and WYPIWYG predictions using the former ones as "experimental" data. a) Tensile Kirchhoff stresses in Pa versus uniaxial (longidutinal) logarithmic strains. b) Transverse strains versus longitudinal strains. c) Energy derivative components ω' in Pa versus deviatoric longitudinal strains: prescribed (Mooney) and obtained (WYPIWYG) energies. d) Volumetric stored energy derivative: prescribed (Hartmann and Neff) and obtained (WYPIWYG) energies.

7.5 Gent model

The Gent stored energy function is [64]

$$\Psi = \mathcal{U}\left(E^v\right) + \psi\left(I_1^d\right) = \mathcal{U}\left(E^v\right) - \frac{\mu J_m}{2}\ln\left(1 - \frac{I_1^d - 3}{J_m}\right) \tag{93}$$

where $\mu = 6000\,\mathrm{Pa}$ and $J_m = 80$ are the material parameter values we have chosen. This model does not admit a Valanis-Landel decomposition which is a basic hypothesis of our proposal. In Figure 10 we show the predictions of the Gent model and the associated stored energy derivatives; in the case of Gent's model the function ψ' was obtained for the uniaxial test at hand. It

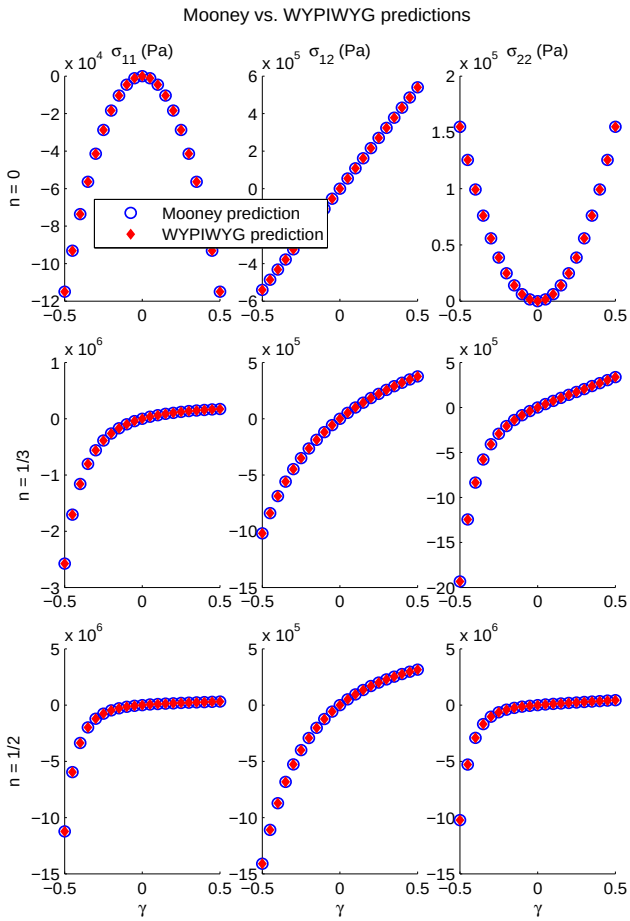

Fig. 7 Predictions for the deformation gradient given in Eq. (90) using the compressible Mooney/Hartmann-Neff model and predictions obtained using the WYPIWYG model using the stored energies of Figure 6. First row: predictions for components σ_{11}, σ_{12}, σ_{22} (Pa) versus γ for $n = 0$ (simple shear) in Eq. (90). Second row: predictions for $n = 1/3$. Third row: predictions for $n = 1/2$.

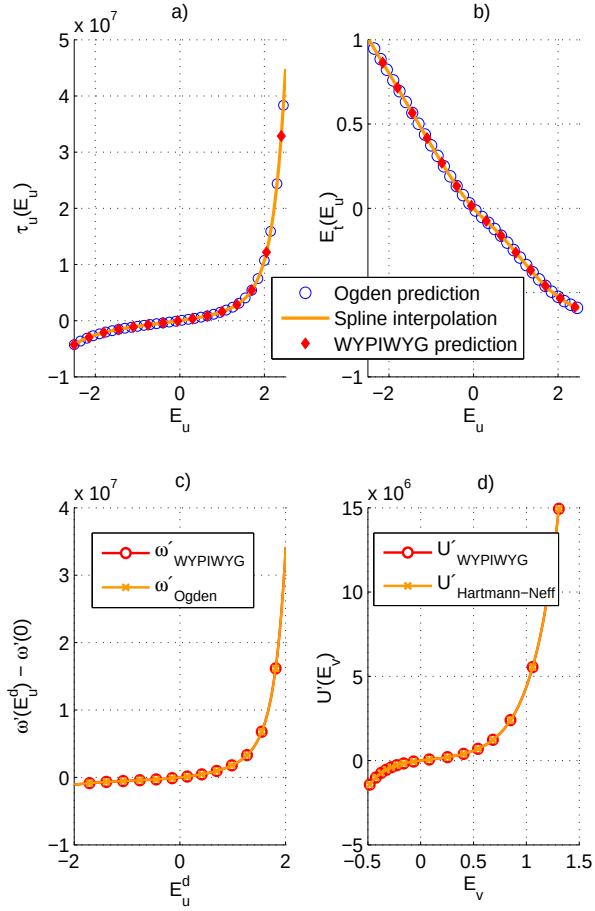

Fig. 8 Compressible Ogden/Hartmann–Neff model predictions for the uniaxial test and WYPIWYG predictions using the former ones as "experimental" data. a) Tensile Kirchhoff stresses in Pa versus uniaxial (longitudinal) logarithmic strains. b) Transverse strains versus longitudinal strains. c) Energy derivative components ω' in Pa versus deviatoric longitudinal strains: prescribed (Ogden) and obtained (WYPIWYG) energies. d) Volumetric stored energy derivative: prescribed (Hartmann and Neff) and obtained (WYPIWYG) energies.

is seen that as in the previous cases the WYPIWYG model is capable of capturing the stress-strain behavior during the uniaxial test.

In Figure 11, the deformation gradients given by Eq. (90) are again imposed to both models. However, in this case we have limited the exponent n to $n = 1/5$ due to the asymptotic behavior of the Gent model. As mentioned the Gent model does not fulfill the Valanis-Landel decomposition. However, for moderate large deformations the Valanis-Landel decomposition is an adequate approximation. The predictions shown in Figure 11 are in line with this observation. Even though Gent's model is not built on the Valanis-Landel decomposition, our WYPIWYG model is able to capture the deformations predicted by Gent's model to a very high accuracy for moderately large deformations.

7.6 Predictions for the Blatz and Ko experiments

We now show the performance of the WYPIWYG approach to predict the behavior measured by the experiments from Blatz-Ko [65] on a polyurethane foam, which is a highly nonlinear compressible material. For this purpose, the data from both the uniaxial tension and equibiaxial tension tests are prescribed and the energy function derivatives ω' and $\mathcal{U}'$ are computed as described in this paper. We have considered that E_w (E_s)

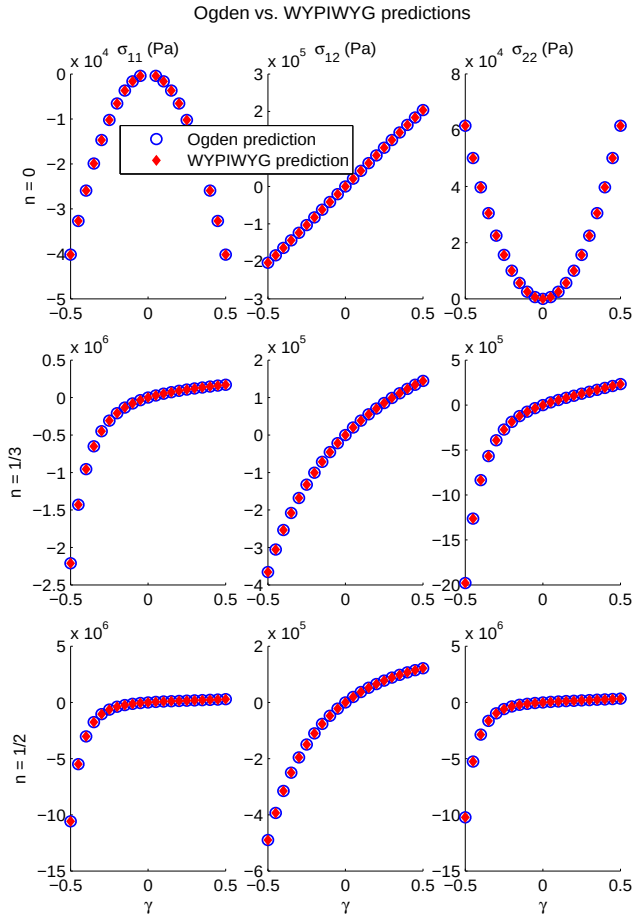

Fig. 9 Predictions for the deformation gradient given in Eq. (90) using the compressible Ogden/Hartmann–Neff model and predictions obtained using the WYPIWYG model using the stored energies of Figure 8. First row: predictions for components σ_{11}, σ_{12}, σ_{22} (Pa) versus γ for $n = 0$ (simple shear) in Eq. (90). Second row: predictions for $n = 1/3$. Third row: predictions for $n = 1/2$.

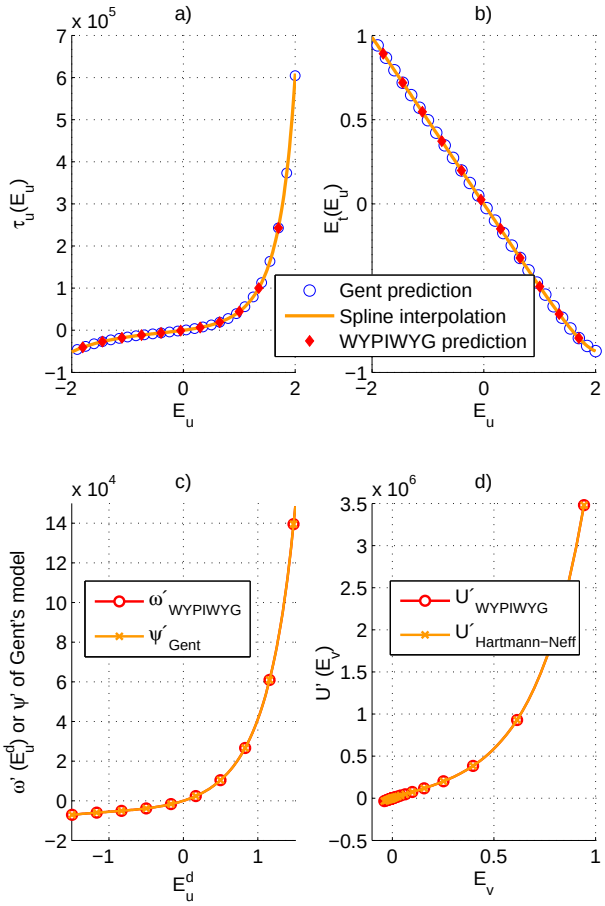

Fig. 10 Compressible Gent/Hartmann–Neff model predictions for the uniaxial test and WYPIWYG predictions using the former ones as "experimental" data. a) Tensile Kirchhoff stresses in Pa versus uniaxial (longidutinal) logarithmic strains. b) Transverse strains versus longitudinal strains. c) Energy derivative components ω' ot ψ' in Pa versus deviatoric longitudinal strains: prescribed (Gent) and obtained (WYPIWYG) energies. d) Volumetric stored energy derivative: prescribed (Hartmann and Neff) and obtained (WYPIWYG) energies.

is an odd function. In Figures 12a and 12b we show the averaged values (the circles in Figure 12) given by Blatz-Ko [65] for the performed experiments, conveniently converted from Figures 13, 14, 21 and 22 of Ref. [65]. This experimental data, slightly smoothed, was captured by the computed stored energy terms, whose derivatives are given in Figures 12c and 12d. These stored energies fully determine the material behavior in any loading situation if the material fulfills the constitutive hypothesis of isotropy and Valanis-Landel decoupling.

We now proceed to predict the behavior of the material for strip-biaxial (plane strain) experiments. In this case the principal deformation is given in axis 1, i.e. $E_s \equiv E_1$. Axis 2 has a vanishing strain $E_2 = 0$ and the thickness reduction is $E_w \equiv E_3$. We can perform the predictions using a finite element. However, since this is an homogeneous deformation it is more straightforward and instructive to solve directly the nonlinear equilibrium equations. The volumetric and deviatoric logarithmic strains are

$$\begin{cases} E^v = E_s + E_w \\ E^d_s = \frac{2}{3}E_s - \frac{1}{3}E_w \\ E^d_2 = -\frac{1}{3}\left(E_s + E_w\right) \\ E^d_w = \frac{2}{3}E_w - \frac{1}{3}E_s \end{cases} \tag{94}$$

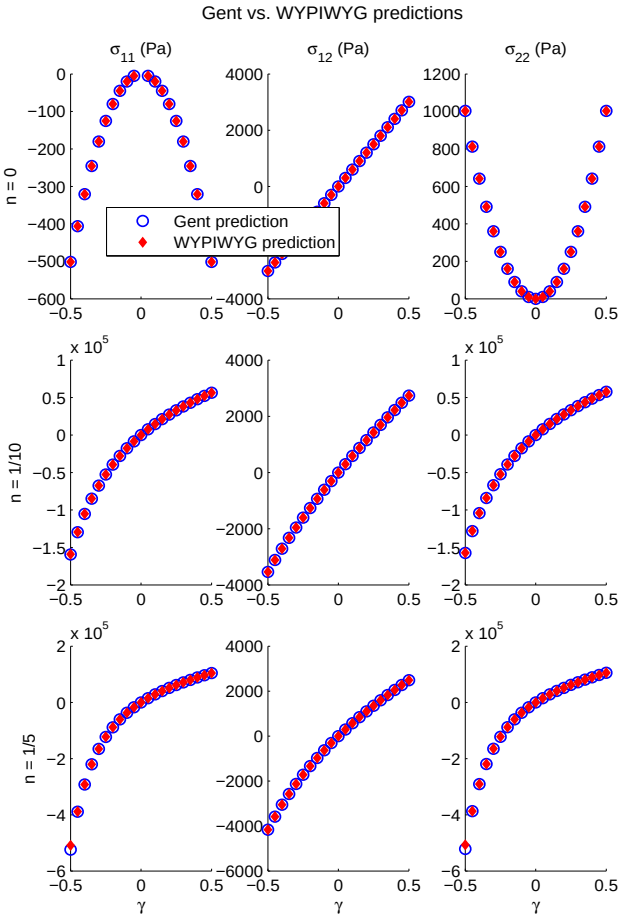

Fig. 11 Predictions for the deformation gradient given in Eq. (90) using the compressible Gent/Hartmann–Neff model and predictions obtained using the WYPIWYG model using the stored energies of Figure 10. First row: predictions for components σ_{11}, σ_{12}, σ_{22} (Pa) versus γ for $n = 0$ (simple shear) in Eq. (90). Second row: predictions for $n = 1/10$. Third row: predictions for $n = 1/5$.

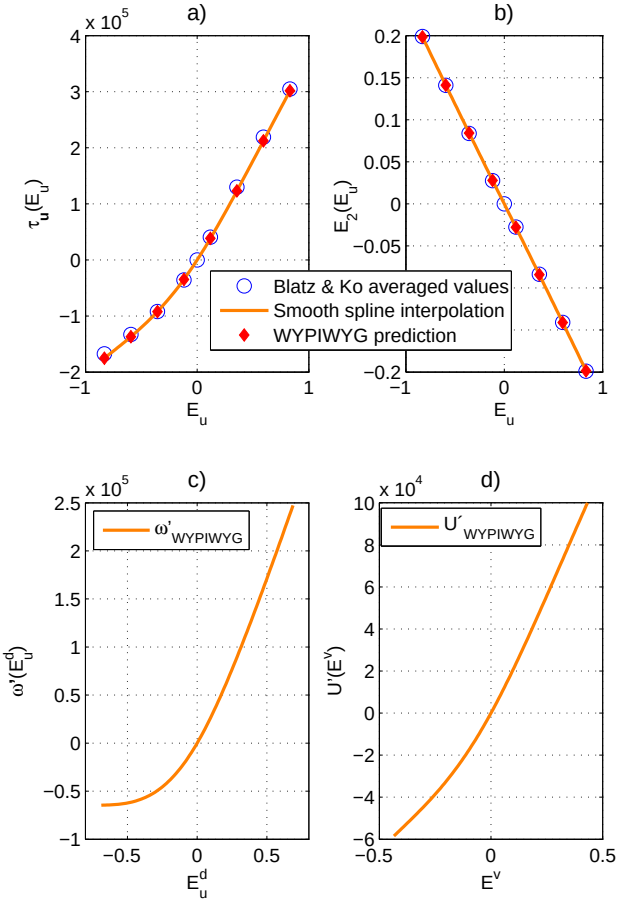

Fig. 12 Determination of the stored energies of polyurethane foam from the Blatz and Ko experimental data. The circles are the averaged data for the experimentes given by Blatz and Ko. The diamonds correspond to the WYPIWYG predictions using the computed stored energies. a) Kirchhoff stress in Pa as a function of the uniaxial strain. b) Transverse strains. c) Computed ω' in units of J / m^3 ≡ Pa. c) Computed volumetric stored energy derivative $\mathcal{U}'$ in Pa.

In order to determine either $E_w\,(E_s)$, or alternatively $E_s\,(E_w)$, we use the boundary condition $\tau_w = 0$ to obtain the nonlinear equation

$$\begin{aligned}&\tfrac{2}{3}\omega'\left(\tfrac{2}{3}E_w - \tfrac{1}{3}E_s\right) - \tfrac{1}{3}\omega'\left(-\tfrac{1}{3}\left(E_s + E_w\right)\right)\\ &-\tfrac{1}{3}\omega'\left(\tfrac{2}{3}E_s - \tfrac{1}{3}E_w\right) + \mathcal{U}'\left(E_s + E_w\right) = 0\end{aligned} \qquad (95)$$

which can be solved for E_w by a Newton-Raphson scheme given a value of E_s. Once the relation $E_w\,(E_s)$ is known, the strains in Eq. (94) are known and we can compute the main stresses by a similar equilibrium equation in Axis 1.

In Figure 13 we show the predictions given by the WYPIWYG model for the strip-biaxial experiments on the same material using the stored energy densities of Figure 12. The predictions for the strip-biaxial experiments are presented against averaged experimental data from Blatz and Ko (Figures 17 and 18 of Ref. [65]). It is seen in Figure 13a that the stresses are accurately predicted by the WYPIWYG formulation, since the error observed is of the order of the experimental errors given in Reference [65]. In Figure 13b we show the predicted transverse strains (thickness reduction) against the longitudinal ones. The observed discrepancies are also in the order of some estimated experimental errors for these quantities, see Figures 22 and 24 of Ref. [65] and note that we plot logarithmic measures.

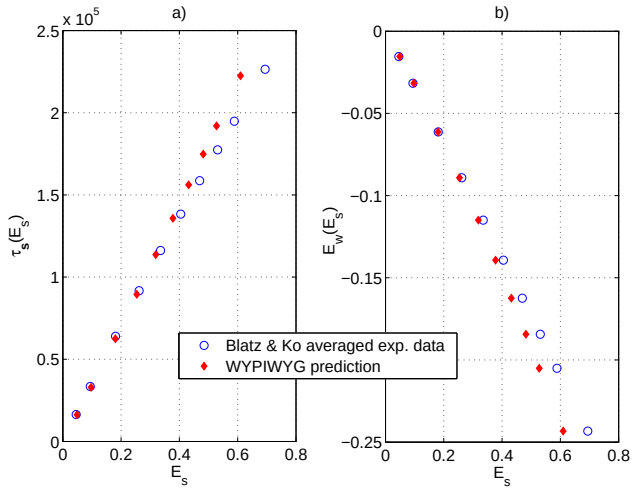

Fig. 13 Predictions of the strip-biaxial experiments from Blatz and Ko using the stored energy density derivatives of Figures 12a and 12b. a) Kirchhoff stresses (Pa) versus longitudinal logarithmic strains. b) Transverse strains (thickness contraction) as a function of longitudinal strains.

7.7 Recovery of the incompressible formulation

In order to show that the (quasi-)incompressible model of Sussman and Bathe is recovered as a particular case, we modify the transverse strains and set $E_2(E_1) = -\nu E_1$ with different values of ν. The case of $\nu \to 0.5$ corresponds to the incompressible formulation. In Figure 14 we show the predictions and stored energy density derivatives for the Ogden model with modified transverse strains as to obtain a constant ν for values from $\nu = 0$ to $\nu = 0.499$. It is seen in Figures 14a and 14b that the prescribed stress-strain uniaxial behavior is still captured. Remarkably Figure 14a shows that the uniaxial stress-strain behavior is exactly captured in all cases. However, it is seen in Figure 14d that the stored energy derivative approaches the values $\mathcal{U}'' \to \infty$, and the volumetric strains $E^v \to 0$ as $\nu \to 0.5$, i.e. they approach the quasi-incompressible case. Note that even though the largest change is in $\mathcal{U}'$, the function ω' also changes with ν so the predicted stress-strain curve given in Figure 14a is "exactly" the same regardless of the ν value; only the predictions in Figure 14b change to accommodate the varying Poisson ratio.

It is well known that incompressibility is frequently imposed in finite element procedures through a penalty volumetric stored energy density. However, because the range of deformations is large and the change in the relative volumetric stiffness may be large, this method frequently results in a too weak imposition of the incompressibility constraint at moderate strains or in numerical conditioning problems at very large strains. The

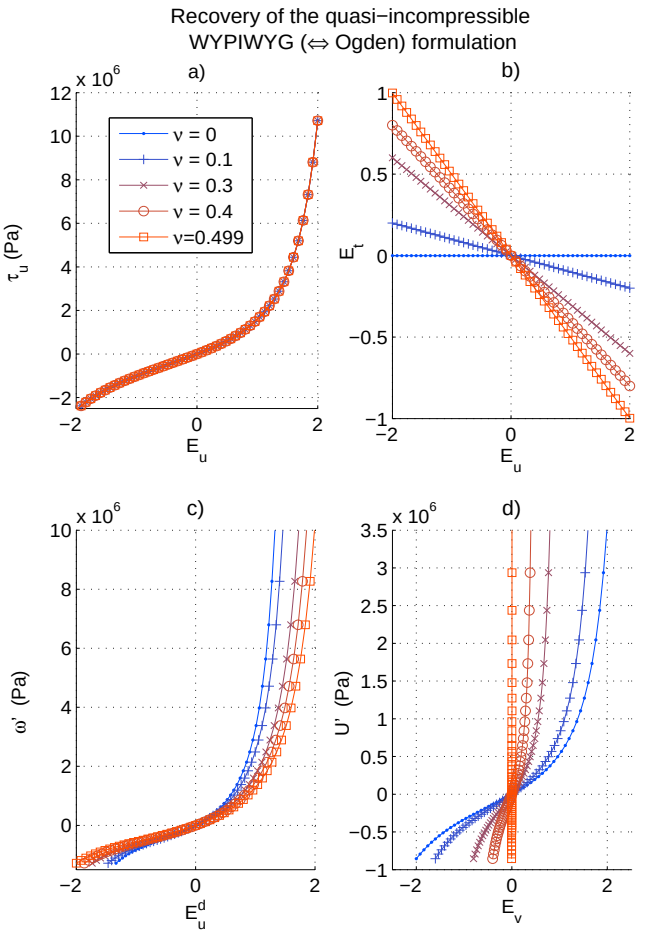

Fig. 14 Determination of the stored energies with modified transverse strains approaching the quasi-incompressible behavior. a) Kirchhoff stress in Pa as a function of the uniaxial strain; uniaxial data from the example using Ogden's model. b) Transverse strains (modified to obtain different ν values). c) Computed derivatives of the stored energy density components ω' in units of $\mathrm{J}/\mathrm{m}^3 \equiv \mathrm{Pa}$. d) Computed volumetric stored energy density derivatives $\mathcal{U}'$ in Pa.

present formulation also allows for an adequate imposition of the incompressibility constraint at all deformation levels simply prescribing a constant value of ν close enough to 0.5 in the transverse strains.

7.8 Plate with a hole using the Ogden model and the WYPIWYG approach

As a demostrative example of the possibilities of the WYPIWYG approach in finite element simulations, we analyze a plate with a hole using our in-house finite element code Dulcinea. This example, with different constitutive models has been used in Refs. [48, 53, 54, 68]. The plate has initial dimensions of $l_0 \times h_0 = 32 \times 16\,\mathrm{mm}^2$ and an inner hole of radius $r_0 = 4\,\mathrm{mm}$.

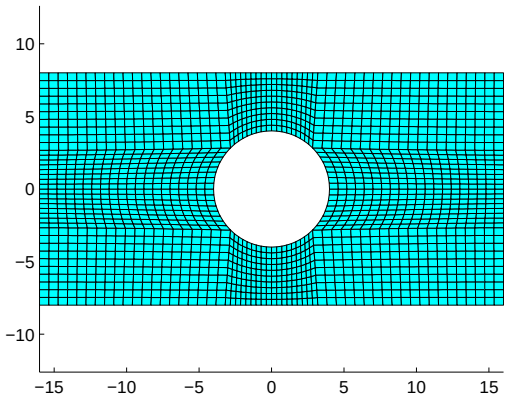

Fig. 15 Rectangular plate with a concentric hole: undeformed finite element mesh employing quadratic elements with full integration.

The material data is the same as that used in the previous Ogden example. We have performed two analyses. One using the compressible Ogden/Hartmann–Neff model and one using our WYPIWYG approach capturing the Ogden/Hartmann–Neff uniaxial data, i.e. we use the stored energy densities of Figures 8c and 8d. The finite element mesh consists of 9-node plane strain quadratic elements with full integration. The prescribed displacement using a penalty approach is of 10 mm imposed at each lateral end in 10 proportional paths (i.e. 2 mm per step).

In Figure 16 we show the von Mises stress distributions and the pressure distributions for both models, along with the deformed meshes at the end of the analysis. As it could have been predicted from the previous examples, no difference can be observed in the results given by both models. This is a consequence of the WYPIWYG model ability to capture the behavior of both the Ogden and the Hartmann–Neff models in any loading situation. Note that we have used the Ogden/Hartmann-Neff model as to clearly show that if this model were exactly predicting the behavior of a real material, we would have exactly (again, numerically speaking) captured the behavior of that material in any loading situation. Of course this conclusion applies to any other model or actual material if the hypotheses of hyperelasticity, isotropy and Valanis-Landel decomposition hold.

Furthermore, in Table 1 we present the relative convergences of both models obtained in a characteristic step. This table shows that indeed the iterations of both models are almost identical; note that only the force residual at iteration 3 and the energy residual at iteration 4 present a difference in the 5 digits shown in the numbers of the table. This should not be a surprise because as repeatedly commented throughout the paper, the numerical values of the energies of both models in any loading situation are also almost identical.

This example has been computed using one processor of a 2011 Windows-PC with Dulcinea running as a 32-bit fortran90 Pentium application. Under these conditions the Ogden/Hartmann–Neff model needed 91 seconds (elapsed time), whereas the WYPIWYG formulation needed 110 seconds. We attribute the difference mainly to the retrieval and addressing operations of the spline coefficients in order to compute the stresses and constitutive tangent. Whereas the material parameters for the Ogden/Hartmann–Neff model are given explicitly to the program, the WYPIWYG computational time includes also the initial determination of the stored energies from uniaxial data. However, this initial determination took less than one second.

Relative convergence rates of the plate-with-a-hole problem. Step 7/10		
	Ogden/Hartmann–Neff model	
Iter	Force residual	Energy residual
1	$1.000E+00$	$1.000E+00$
2	$1.339E-03$	$4.449E-06$
3	$5.441E-06$	$2.542E-11$
4	$2.998E-11$	$3.069E-21$
	WYPIWYG model	
Iter	Force residual	Energy residual
1	$1.000E+00$	$1.000E+00$
2	$1.339E-03$	$4.449E-06$
3	$5.443E-06$	$2.542E-11$
4	$2.998E-11$	$3.071E-21$

Table 1 Convergence rates for both the Ogden/Hartmann–Neff model and the WYPIWYG model

8 Conclusions

WYPIWYG hyperelasticity differs from traditional models in that the shape of the stored energy is not assumed beforehand, in that there are no material parameters and in that no optimization algorithms to obtain those parameters are needed. The stored energies are numerically computed to the desired precision solving the differential equations of the tests. These tests uniquely (numerically speaking) define the stored energy under the constitutive assumptions. In this work we have presented a WYPIWYG procedure to numerically compute the stored energy for compressible isotropic materials fulfilling the Valanis-Landel hypothesis. We have

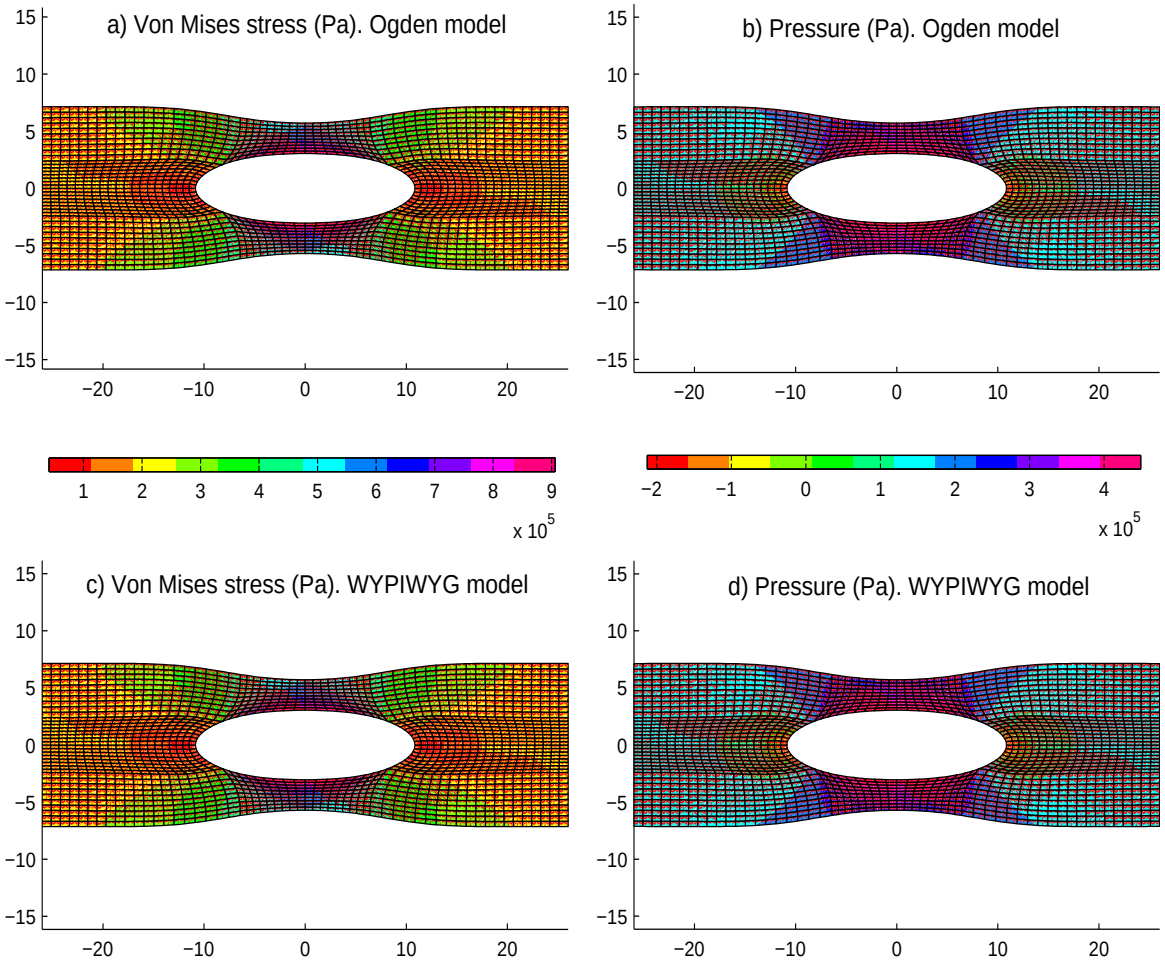

Fig. 16 Rectangular plate with a concentric hole. Deformed meshes and stresses. a) Von Mises stress distribution (Pa) for the Ogden/Hartmann-Neff model. b) Pressure distribution (Pa) for the Ogden/Hartmann-Neff model. c) Von Mises stress distribution for the WYPIWYG model. d) Pressure distribution for the WYPIWYG model

shown that the model is capable of capturing analytical models using the Valanis-Landel decomposition and of predicting the behavior observed in the experiments of Blatz and Ko. Furthermore, we have shown that the quasi-incompressible formulation is naturally recovered.

Because we understand WYPIWYG models as a natural extension of the infinitesimal framework to large strains, we have motivated the formulation in the small strain setting and have justified the number of tests needed to uniquely define such materials, an issue frequently not clear in the literature [8], [56]. Furthermore, we have also explained the way to convert data from equibiaxial and confined compression tests to the standard data of an equivalent uniaxial tension-compression curve, which can be used as the standardized input in finite element procedures. The efficiency of WYPIWYG procedures in general finite element simulations is parallel to that of traditional models not only in the case of compressible isotropy presented herein but also in the case of anisotropy [48, 54].

Acknowledgements

Partial financial support for this work has been given by grants DPI2011-26635 and DPI2015-69801-R from the Dirección General de Proyectos de Investigación of the Ministerio de Economía y Competitividad of Spain. F.J. Montáns also acknowledges the support of the Department of Mechanical and Aerospace Engineering of University of Florida during the sabbatical period in which this paper was finished and that of the Ministerio

de Educación, Cultura y Deporte of Spain for the financial support for that stay under grant PRX15/00065.

References

1. Landel RF, Nielsen LE (1993) Mechanical properties of polymers and composites. CRC Press, Boca Ratón.
2. Ward IM, Hadley DW (1993). An Introduction to the Mechanical Properties of Solid Polymers. John Wiley & Sons Ltd, Chichister.
3. Ogden RW (1997) Nonlinear Elastic Deformations. Dover, New York.
4. Holzapfel GA (2000). Nonlinear Solid Mechanics. John Wiley & Sons Ltd, Chichester.
5. Humphrey JD (2013). Cardiovascular Solid Mechanics: Cells, Tissues, and Organs. Springer, New York.
6. Fung YC (1993). A First Course in Continuum Mechanics. Prentice-Hall, New Jersey.
7. Twizell EH, Ogden RW (1983) Non-linear optimization of the material constants in Ogden's stress-deformation function for incompressinle isotropic elastic materials. J Aust Math Soc B 24(04):424–434.
8. Ogden RW, Saccomandi G, Sgura I (2004) Fitting hyperelastic models to experimental data. Comput Mech 34(6):484–502.
9. Kakavas PA (2000) A new development of the strain energy function for hyperelastic materials using a logarithmic strain approach. J Appl Polym Sci 77:660–672.
10. Pancheri FQ, Dorfmann L (2014) Strain-controlled biaxial tension of natural rubber: new experimental data. Rubber Chem Technol 87(1):120–138.
11. Palmieri G, Sasso M, Chiappini G, Amodio D (2009) Mullins effect characterization of elastomers by multiaxial cyclic tests and optical experimental methods. Mech Mater 41(9):1059–1067.
12. Urayama K (2006). An experimentalist's view of the physics of rubber elasticity. J Polym Sci Polym Phys 44:3440–3444.
13. Khajehsaeid H, Arghavani J, Naghdabadi R (2013) A hyperelastic constitutive model for rubber-like materials. Eur J Mech A-Solid, 38, 144–151.
14. Lopez-Pamies O. A new I_1-based hyperelastic model for rubber elastic materials (2010) CR Mechanique 338(1):3–11.
15. Maeda N, Fujikawa M, Makabe C, Yamabe J, Kodama Y, Koishi M (2015) Performance evaluation of various hyperelastic constitutive models of rubbers. In: Marvalova B and Petrikova I (eds), Constitutive Models for Rubbers IX, CRC Press, pp 271–277.
16. Steinmann P, Hossain M, Possart G (2012) Hyperelastic models for rubber-like materials: consistent tangent operators and suitability for Treloar's data. Arch Appl Mech 82:1183–1217.
17. Bechir H, Chevalier L, Chaouche M, Boufala K (2006) Hyperelastic constitutive model for rubber-like materials based on the first Seth strain measures invariant. Eur J Mech A-Solid 25(1):110–124.
18. Gendy AS, Saleeb AF (2000) Nonlinear material parameter estimation for characterizing hyperelastic large strain models. Comput Mech 25(1):66–77.
19. Stumpf PT, Marczak RJ (2010) Optimization of constitutive parameters for hyperelastic models satisfying the Baker-Ericksen inequalities. In: Dvorkin E, Goldschmit M, Storti M (eds). Mecanica Computational XXIX, Asociación Argentina de Mecánica Computacional, Buenos Aires, pp 2901–2916.
20. Bradley GL, Chang PC, McKenna GB (2001) Rubber modeling using uniaxial test data. J Appl Polym Sci 81(4):837–848.
21. Hariharaputhiran H, Saravanan U (2016). A new set of biaxial and uniaxial experiments on vulcanized rubber and attempts at modeling it using classical hyperelastic models. Mech Mater 92:211–222.
22. Mansouri MR, Darijani H (2014) Constitutive modelling of isotropic hyperelastic materials in an exponential framework using a self-contained approach. Int J Solid Struct 51: 4316–4326.
23. Grytz R, Meschke G, Jonas JB, Downs JC (2016) Glaucoma and Structure-Based Mechanics of the Lamina Cribrosa at Multiple Scales. In: Kassab GS, Sacks MS (eds), Structure-Based Mechanics of Tissues and Organs, Springer, New York, pp 93–122.
24. Moerman KM, Simms CK, Nagel T (2016) Control of tension–compression asymmetry in Ogden hyperelasticity with application to soft tissue modelling. J Mech Beh Biomed Mater 56:218–228.
25. Holzapfel GA (2006). Determination of material models for arterial walls from uniaxial extension tests and histological structure. J Theor Biol 238(2):290–302.
26. Li D, Robertson AM (2009). A structural multimechanism constitutive equation for cerebral arterial tissue. Int J Solid Struct 46:2920–2928.
27. Shearer T (2015). A new strain energy function for the hyperelastic modelling of ligaments and tendons based on fascicle microstructure. J Biomech 48(2):290–297.
28. Holzapfel GA, Niestrawska JA, Ogden RW, Reinisch AJ, Schriefl AJ (2015). Modelling non-symmetric collagen fiber dispersion in arterial walls. J Roy Soc Interface 12:20150188.
29. Itskov M, Aksel N (2004) A class of orthotropic and transversely isotropic hyperelastic constitutive models based on a polyconvex strain energy function. Int J Solid Struct 41(14): 3833–3848.
30. Angeli S, Panayiotou C, Psimolophitis E, Nicolaou M, Constantinides C (2015). Uniaxial Stress-Strain Characteristics of Elastomeric Membranes: Theoretical Considerations, Computational Simulations, and Experimental Validation. Mech Adv Mater Struct 22(12): 996–1006.
31. Chen H, Zhao X, Lu X, Kassab GS (2016) Microstructure-Based Constitutive Models for Coronary Artery Adventitia. In: Kassab GS, Sacks MS (eds), Structure-Based Mechanics of Tissues and Organs, Springer, New York, pp 225–248.
32. Pierce DM, Maier F, Weisbecker H, Viertler C, Verbrugghe P, Famaey N, Holzapfel GA (2015) Human thoracic and abdominal aortic aneurysmal tissues: damage experiments, statistical analysis and constitutive modeling. J Mech Beh Biomed Mater 41:92–107.
33. Cooney GM, Moerman KM, Takaza M, Winter DC, Simms CK (2015). Uniaxial and biaxial mechanical properties of porcine linea alba. J Mech Beh Biomed Mater 41:68–82.
34. Santamaría VA, Siret O, Badel P, Guerin G, Novacek V, Turquier F, Avril S (2015) Material model calibration from planar tension tests on porcine linea alba. J Mech Beh Biomed Mater 43:26–34.
35. Sacks MS (2003). Incorporation of experimentally-derived fiber orientation into a structural constitutive model for planar collagenous tissues. J Biomech Engrg 125(2):280–287.
36. Natali AN, Carniel EL, Pavan PG, Dario P, Izzo I (2006) Hyperelastic models for the analysis of soft tissue mechanics: definition of constitutive parameters. In:

Biomedical Robotics and Biomechatronics, IEEE, pp 188–191.
37. Tricerri P, Dedè L, Gambaruto A, Quarteroni A, Sequeira A (2016) A numerical study of isotropic and anisotropic constitutive models with relevance to healthy and unhealthy cerebral arterial tissues. Int J Engrg Sci 101:126–155.
38. Cortes DH, Elliott DM (2016) Modeling of Collagenous Tissues Using Distributed Fiber Orientations. In: Kassab GS, Sacks MS (eds), Structure-Based Mechanics of Tissues and Organs, Springer, New York, pp 15–40.
39. Gasser TC. Histomechanical Modeling of the Wall of Abdominal Aortic Aneurysm (2016) In: Kassab GS, Sacks MS (eds), Structure-Based Mechanics of Tissues and Organs, Springer, New York, pp 57–78.
40. Kamenskiy AV, Pipinos II, Dzenis YA, Phillips NY, Desyatova AS, Kitson J, Bowen R, MacTaggart JN (2015) Effects of age on the physiological and mechanical characteristics of human femoropopliteal arteries. Acta Biomater 11:304–313.
41. Lee LC, Wenk J, Klepach D, Kassab GS, Guccione JM. Structural-BasedModels of Ventricular Myocardium (2016) In: Kassab GS, Sacks MS (eds), Structure-Based Mechanics of Tissues and Organs, Springer, New York, pp 249–264.
42. Fehervary H, Smoljkić M, Sloten JV, Famaey N (2016) Planar biaxial testing of soft biological tissue using rakes: a critical analysis of protocol and fitting process. J Mech Beh Biomed Mater 61:135–151.
43. Valanis KC, Landel RF. The stored energy of a hyperelastic material in terms of the extension ratios (1967) J Appl Phys 38:2997.
44. Sussman T, Bathe KJ (2009) A model of incompressible isotropic hyperelastic material behavior using spline interpolations of tension-compression test data. Commun Num Meth Engrg 25(1):53–63.
45. Kearsley EA, Zapas LJ. Some Methods of Measurement of an Elastic Strain Energy Function of the Valanis-Landel Type (1980) J Rheol 24:483.
46. ADINA Theory and Modelling Guide, ARD 12-8 (2012). ADINA R&D, Watertown, 2012.
47. Latorre M, Montáns FJ. Extension of the Sussman–Bathe spline-based hyperelastic model to incompressible transversely isotropic materials. Comput Struct, 122:13–26, 2013.
48. Latorre M, Montáns FJ. What-You-Prescribe-Is-What-You-Get orthotropic hyperelasticity. Comput Mech, 53(6): 1279–1298, 2014.
49. Latorre M, Montáns FJ (2014) On the interpretation of the logarithmic strain tensor in an arbitrary system of representation. Int J Solid Struct 51(7):1507–1515.
50. Fiala Z (2015) Discussion of "On the interpretation of the logarithmic strain tensor in an arbitrary system of representation" by M. Latorre and F.J. Montáns Int J Solid Struct 56–57:290–291.
51. Latorre M, Montáns FJ (2015) Response to Fiala's comments on "On the interpretation of the logarithmic strain tensor in an arbitrary system of representation". Int J Solid Struct 56–57:292.
52. Neff P, Eidel B, Martin RJ (2015) Geometry of logarithmic strain measures in solid mechanics. ArXiv:1505.02203 [MathDG]
53. Latorre M, Montáns FJ (2015) Anisotropic finite strain viscoelasticity based on the Sidoroff multiplicative decomposition and logarithmic strains. Comput Mech 56:503–531.
54. Latorre M, Montáns FJ (2016) Fully anisotropic finite strain viscoelasticity based on a reverse multiplicative decomposition and logarithmic strains. Comput Struct 163:56–70.
55. Miñano M, Montáns FJ (2015) A new approach to modeling isotropic damage for Mullins effect in hyperelastic materials. Int J Solid Struct 67-68:272–282, 2015.
56. Latorre M, De Rosa E, Montáns FJ (2016) Understanding the need of the compression branch to characterize hyperelastic materials. Under review.
57. Latorre M, Romero X, Montáns FJ (2016) The relevance of transverse deformation effects in modeling soft biological tissues. Under review.
58. Romero X, Latorre M, Montáns FJ (2016) Determination of the WYPIWYG strain energy density of skin through finite element analysis of the experiments on circular specimens. Under review.
59. Bower, A. F. (2009) Applied Mechanics of Solids. CRC press, Boca Ratón.
60. Ogden RW (1972) Large deformation isotropic elasticity-on the correlation of theory and experiment for incompressible rubberlike solids. P Roy Soc London A Math 326(1567):565–584.
61. Ogden RW (1973) Large deformation isotropic elasticity-on the correlation of theory and experiment for incompressible rubberlike solids. Ruber Chem Technol 46(2): 398–416. 1973.
62. Mooney M (1940) A theory of large elastic deformation. J Appl Phys 11:582–592.
63. Hartmann S, Neff P (2003). Polyconvexity of generalized polynomial-type hyperelastic strain energy functions for near-incompressibility. Int J Solid Struct 40(11):2767-2791.
64. Gent AN (1996) A new constitutive relation for rubber. Rubber Chem Technol 69(1): 59–61.
65. Blatz PJ, Ko WL (1962) Application of finite elastic theory to the deformation of rubbery materials. T Soc Rheol 223–251.
66. Latorre M, Montáns FJ (2016) Stress and strain mapping tensors and general work-conjugacy in large strain continuum mechanics. Appl Math Model 40(5-6):3938–3950.
67. Latorre M, Montáns FJ (2015) Material-symmetries congruency in transversely isotropic and orthotropic hyperelastic materials. Eur J Mech A-Solid 53:99-106.
68. Caminero MA, Montáns FJ, Bathe KJ (2011) Modeling large strain anisotropic elasto-plasticity with logarithmic strain and stress measures. Comput Struct 89(11):826-843.
69. Dierckx P (1993). Curve and Surface Fitting with Splines. Oxford University Press, Oxford.
70. Eubank RL (1999). Nonparametric Regression and Spline Smoothing. Marcel Dekker, New York.
71. Weinert HL (2013). Fast Compact Algorithms and Software for Spline Smoothing. Springer, New York.